Ligand isomerism fine-tunes structure and stability in zinc complexes of fused pyrazolopyridines

Amelia M. Swarbrook, Rohan J. Weekes, Jack W. Goodwin, and Chris S. Hawes

Supporting Information

1. X-ray Data Tables
2. Additional Experimental Details
3. Additional Figures
4. UV-Visible and Fluorescence Spectroscopy
5. Thermogravimetric Analysis
6. Gas Adsorption Figures and Data
7. X-ray Powder Diffraction
8. NMR Spectroscopy
9. References

1. X-ray Data Tables

Table S1 Crystal and refinement parameters for **L3 – L6**

Identification code	**L3**	**L4**	**L5**	**L6**
Empirical formula	$C_{11}H_8N_4$	$C_{11}H_8N_4$	$C_{11}H_8N_4$	$C_{11}H_8N_4$
Formula weight	196.21	196.21	196.21	196.21
Temperature/K	150	150	150	150
Crystal system	triclinic	monoclinic	monoclinic	orthorhombic
Space group	P-1	$P2_1/n$	$P2_1/c$	$Pna2_1$
a/Å	7.3682(7)	6.8153(3)	6.9365(3)	10.9868(7)
b/Å	7.3765(7)	18.8138(9)	10.1955(5)	4.5407(3)
c/Å	9.1496(9)	7.7716(4)	12.7905(6)	18.0875(12)
α/°	77.206(4)	90	90	90
β/°	77.592(4)	113.8950(10)	99.2890(10)	90
γ/°	69.480(3)	90	90	90
Volume/Å^3	449.02(8)	911.08(8)	892.70(7)	902.34(10)
Z	2	4	4	4
ρ_{calc}g/cm^3	1.451	1.43	1.46	1.444
μ/mm^{-1}	0.093	0.092	0.094	0.093
F(000)	204	408	408	408
Crystal size/mm^3	0.49 × 0.46 × 0.05	0.41 × 0.15 × 0.09	0.42 × 0.09 × 0.08	0.64 × 0.25 × 0.09
Radiation	MoKα (λ = 0.71073)	MoKα (λ = 0.71073)	MoKα (λ = 0.71073)	MoKα (λ = 0.71073)
2Θ range for data collection/°	5.974 to 55.166	6.13 to 61.078	5.952 to 54.234	7.418 to 61.092
Index ranges	-9 ≤ h ≤ 8, -9 ≤ k ≤ 9, -11 ≤ l ≤ 11	-9 ≤ h ≤ 9, -26 ≤ k ≤ 26, -11 ≤ l ≤ 11	-8 ≤ h ≤ 8, 0 ≤ k ≤ 13, 0 ≤ l ≤ 16	-15 ≤ h ≤ 15, -6 ≤ k ≤ 6, -25 ≤ l ≤ 25
Reflections collected	4514	18810	2003	12599
Independent reflections	2055 [R_{int} = 0.0307, R_{sigma} = 0.0468]	2783 [R_{int} = 0.0370, R_{sigma} = 0.0229]	2003 [R_{int} = 0.0422, R_{sigma} = 0.0251]	2733 [R_{int} = 0.0376, R_{sigma} = 0.0305]
Data/restraints/parameters	2055/0/136	2783/0/136	2003/0/137	2733/1/136
Goodness-of-fit on F^2	1.039	1.133	1.13	1.078
Final R indexes [I>=2σ (I)]	R_1 = 0.0514, wR_2 = 0.1127	R_1 = 0.0540, wR_2 = 0.1281	R_1 = 0.0413, wR_2 = 0.0997	R_1 = 0.0399, wR_2 = 0.0906
Final R indexes [all data]	R_1 = 0.0738, wR_2 = 0.1222	R_1 = 0.0629, wR_2 = 0.1324	R_1 = 0.0480, wR_2 = 0.1032	R_1 = 0.0436, wR_2 = 0.0923
Largest diff. peak/hole / e Å^{-3}	0.29/-0.28	0.34/-0.29	0.21/-0.23	0.25/-0.24
Flack Parameter	n/a	n/a	n/a	-1.7(6)
CCDC No.	2121405	2121406	2121407	2121408

Table S2 Crystal and Refinement Parameters for complexes **1** – **4**

Identification code	**1**	**2**	**3**	**4**
Empirical formula	$C_{26}H_{16}N_6O_4Zn_2$	$C_{16}H_{15}N_4O_3Zn$	$C_{11}H_8N_6O_6Zn$	$C_{11}H_{10}N_6O_7Zn$
Formula weight	607.19	376.69	385.6	403.62
Temperature/K	150	150	150	150
Crystal system	monoclinic	monoclinic	monoclinic	orthorhombic
Space group	$C2/c$	$P2_1/c$	$P2_1/n$	$Pbcn$
a/Å	35.314(4)	15.9545(9)	8.5507(3)	24.908(3)
b/Å	9.6459(10)	9.4496(5)	11.2088(4)	7.1377(7)
c/Å	11.2289(11)	11.2888(5)	13.9264(6)	16.5359(17)
α/°	90	90	90	90
β/°	102.392(3)	110.631(2)	91.2400(10)	90
γ/°	90	90	90	90
Volume/Å^3	3735.9(7)	1592.79(14)	1334.44(9)	2939.8(5)
Z	4	4	4	8
ρ_{calc}g/cm^3	1.08	1.571	1.919	1.824
μ/mm^{-1}	1.314	1.564	1.89	1.725
F(000)	1224	772	776	1632
Crystal size/mm^3	$0.1 \times 0.07 \times 0.03$	$0.14 \times 0.11 \times 0.06$	$0.27 \times 0.26 \times 0.07$	$0.35 \times 0.08 \times 0.02$
Radiation	MoKα ($\lambda = 0.71073$)	MoKα ($\lambda = 0.71073$)	MoKα ($\lambda = 0.71073$)	MoKα ($\lambda = 0.71073$)
2Θ range for data collection/°	6.208 to 52.832	5.456 to 61.106	5.852 to 61.066	5.192 to 53.998
Index ranges	$-44 \leq h \leq 44, -12 \leq k \leq 12, -14 \leq l \leq 14$	$-21 \leq h \leq 22, -12 \leq k \leq 13, -16 \leq l \leq 11$	$-11 \leq h \leq 12, -16 \leq k \leq 16, -19 \leq l \leq 19$	$-27 \leq h \leq 31, -9 \leq k \leq 9, -21 \leq l \leq 21$
Reflections collected	18019	20900	23573	27682
Independent reflections	3827 [R_{int} = 0.1180, R_{sigma} = 0.0814]	4868 [R_{int} = 0.0736, R_{sigma} = 0.0591]	4056 [R_{int} = 0.0269, R_{sigma} = 0.0205]	3202 [R_{int} = 0.0791, R_{sigma} = 0.0456]
Data/restraints/parameters	3827/60/208	4868/0/219	4056/0/217	3202/2/234
Goodness-of-fit on F^2	1.025	1.03	1.058	1.112
Final R indexes [I>=2σ (I)]	R_1 = 0.0514, wR_2 = 0.1219	R_1 = 0.0450, wR_2 = 0.1068	R_1 = 0.0262, wR_2 = 0.0623	R_1 = 0.0549, wR_2 = 0.0991
Final R indexes [all data]	R_1 = 0.0756, wR_2 = 0.1302	R_1 = 0.0779, wR_2 = 0.1202	R_1 = 0.0326, wR_2 = 0.0646	R_1 = 0.0765, wR_2 = 0.1059
Largest diff. peak/hole / e Å^{-3}	0.74/-0.49	1.82/-0.72	0.55/-0.47	0.85/-0.55
CCDC No.	2121409	2121410	2121411	2121412

Table S3 Crystal and Refinement Parameters for **5α**, **5β** and **6**

Identification code	**5α**	**5β**	**6**
Empirical formula	$C_{11}H_{18}N_6O_{11}Zn$	$C_{59}H_{50}N_{26}O_{14}Zn_2$	$C_{28}H_{25}N_{15}O_{12}Zn_2$
Formula weight	475.68	1477.99	894.37
Temperature/K	150	150	150
Crystal system	monoclinic	monoclinic	monoclinic
Space group	$P2_1/c$	$P2_1/c$	$C2/c$
a/Å	6.9228(7)	13.5157(9)	26.481(2)
b/Å	15.0043(14)	23.5974(16)	9.7011(9)
c/Å	17.5340(15)	10.2149(7)	16.5236(15)
α/°	90	90	90
β/°	98.558(2)	109.652(2)	124.005(2)
γ/°	90	90	90
Volume/Å³	1801.0(3)	3068.1(4)	3518.9(6)
Z	4	2	4
ρ_{calc}g/cm³	1.754	1.6	1.688
μ/mm⁻¹	1.438	0.873	1.448
F(000)	976	1516	1816
Crystal size/mm³	$0.32 \times 0.08 \times 0.04$	$0.39 \times 0.12 \times 0.01$	$0.28 \times 0.08 \times 0.02$
Radiation	MoKα (λ = 0.71073)	MoKα (λ = 0.71073)	MoKα (λ = 0.71073)
2Θ range for data collection/°	4.698 to 55.992	4.572 to 52.742	5.948 to 52.878
Index ranges	-9 ≤ h ≤ 9, -19 ≤ k ≤ 19, -23 ≤ l ≤ 20	-16 ≤ h ≤ 16, -29 ≤ k ≤ 29, -12 ≤ l ≤ 12	-33 ≤ h ≤ 33, -12 ≤ k ≤ 12, -20 ≤ l ≤ 19
Reflections collected	23231	61152	25275
Independent reflections	4328 [R_{int} = 0.0953, R_{sigma} = 0.0696]	6257 [R_{int} = 0.1566, R_{sigma} = 0.0974]	3615 [R_{int} = 0.0913, R_{sigma} = 0.0583]
Data/restraints/parameters	4328/1/271	6257/187/574	3615/0/261
Goodness-of-fit on F²	1.144	1.075	1.098
Final R indexes [I>=2σ (I)]	R_1 = 0.0631, wR_2 = 0.1132	R_1 = 0.0939, wR_2 = 0.1304	R_1 = 0.0538, wR_2 = 0.1188
Final R indexes [all data]	R_1 = 0.0953, wR_2 = 0.1220	R_1 = 0.1628, wR_2 = 0.1515	R_1 = 0.0829, wR_2 = 0.1303
Largest diff. peak/hole / e Å⁻³	0.99/-0.89	0.39/-0.40	1.02/-0.54
CCDC No.	2121413	2121414	2121415

2. Additional Experimental Details

Materials and Methods

All reagents and starting materials were purchased from Merck, Fluorochem or Alfa Aesar and used as received. **HL1** and **HL2** are commercially available, but can be conveniently prepared from the corresponding aminopicolines (as described below). NMR spectroscopy was carried out using a Bruker Avance III HD 400 spectrometer operating at 400 MHz for ^{1}H and 101 MHz for ^{13}C. Samples were dissolved in deuterated solvents (Cambridge Isotope Laboratories) and spectra were referenced to residual solvent peaks and/or TMS. Elemental analysis were performed using a Thermo Flash 2000 CHNS analyser, referenced against sulfanilimide. Infrared spectra were recorded using a Thermo Scientific Nicolet iS10 instrument operating in ATR sampling mode. Melting points were recorded in air on a Stuart digital melting point apparatus and are uncorrected. Thermogravimetric analysis was performed with an STA1500 thermal analyser (Thorn Scientific Services), under a nitrogen atmosphere and with a heating rate of 5 °C per minute up to 500 °C. High resolution mass spectra were measured at the EPSRC National Mass Spectrometry Facility at Swansea University, U.K.

Photophysical measurements were carried out using an Agilent Cary 50 Bio spectrophotometer and Agilent Eclipse fluorimeter. All samples were dissolved in spectrophotometric grade solvents (Alfa Aesar) in Starna quartz cuvettes. All UV/Visible and fluorescence titrations were performed in triplicate. Data fitting was carried out on the fluorescence titrations with the non-linear least squares global fitting procedure in ReactLab Equilibria[S1] using a 1M:1L binding model for initial fits followed by testing for additional species where correlated residuals were evident. Association constants are reported as logK (1:1) or logβ (all other stoichiometries) with standard deviations derived from independent collections and fits of at least 3 datasets each.

X-ray powder diffraction patterns were measured with a Bruker D8 Advance diffractometer with Cu-Kα radiation (λ = 1.54178 Å). All samples were mounted on a zero-background silicon single crystal sample holder, with the exception of complex **6** and the methanol-exchanged MOFs **1** and **2** which were measured under solvent in a CTS capillary. All samples were measured at room temperature and compared against the simulated patterns from the single crystal datasets (150 K).

Gas adsorption measurements were performed using a Quantachrome Autosorb iQ using N_2 and CO_2 at N4.5 grade or better. Temperature control was provided by a liquid nitrogen dewar for N_2 measurements and a Julabo recirculating chiller for CO_2 measurements. Samples were activated prior to the adsorption experiment by soaking in methanol for 3 days, exchanging for fresh solvent every 12 hours. Initial activation was performed at 100 °C under dynamic vacuum provided by a rotary oil pump followed by soaking under high vacuum provided by a turbomolecular pump at 100 °C for 12 hours.

X-ray Crystallography

Crystal and refinement parameters are given in Tables S1-S3 (ESI). All data were collected with a Bruker D8 Quest ECO diffractometer using Mo Kα radiation (λ = 0.71073 Å). Crystals were mounted on Mitegen micromounts in NVH immersion oil and cooled to 150 K during the collections using an Oxford cryostream. Data collection and reduction were controlled using the Bruker APEX-3 suite of programs.[S2] Multi-scan absorption corrections were applied using SADABS.[S3] All data were solved using the intrinsic phasing routine within SHELXT[S4] and refined on F^2 using full-matrix least squares procedures with SHELXL[S5] within the OLEX-2 package.[S6] Crystals of **L4** tend to crystallise as non-merohedral twins, and for this dataset the overlapping domains were indexed using CELL_NOW[S7] and the intensity data for the two domains were scaled and merged with TWINABS,[S8] with the final refinements being performed on the HKLF5 datasets. Hydrogen atoms were generally assigned in calculated positions with isotropic displacement parameters derived from the isotropic equivalent of

their carrier atoms, except in the case of hydrogen bonding groups if the hydrogen atom positions could be unambiguously determined from the Fourier residuals. Specific refinement strategies are outlined in the refine_special_details sections of the combined cif. The SMTBX solvent masking routine[S9] was used to account for regions of continuous electron density representing heavily disordered solvent within the structure of complex **1**. The solvation for this species was established from TGA and elemental analysis results suggesting an overall formula of $[Zn_2(\textbf{L1})_2(bpdc)]\cdot 1.5DMF\cdot 3H_2O$ (90 e⁻/formula unit, *vs.* 73 e⁻ calc.). The crystals of complex **5β** were unavoidably poor quality with weak scattering behaviour and a heavily disordered component (Figure S1); this structure is intended as a connectivity model only for the minor crystalline phase. CCDC 2121405-2121415.

Synthesis of HL1/HL2

Both **HL1** and **HL2** are commercially available but can be conveniently prepared from the corresponding aminopicolines. In a typical procedure, a 250 mL 3-necked flask fitted with a reflux condenser was charged with 3-amino-2-methylpyridine (3.00 g, 27.8 mmol), potassium acetate (2.73 g, 27.8 mmol), and anhydrous toluene (90 mL) under a nitrogen atmosphere. Acetic anhydride (13 mL, 140 mmol) was added to the stirring mixture, and the suspension heated to reflux. After 30 minutes, isoamyl nitrite (7.7 mL, 57 mmol) was added dropwise and reflux maintained for a further 22 hours. Upon cooling to room temperature, the solids were filtered and washed with toluene (2×20 mL). The combined filtrate was concentrated by distillation, giving the crude N-acetyl intermediate. The resulting brown oil was dissolved in 25% aqueous hydrochloric acid (40 mL) and heated under reflux for 2 hours. The reaction was cooled to room temperature and taken to pH 9 with aqueous ammonia. The solution was washed with toluene (50 mL), and the organic layer discarded. The aqueous solution was extracted with dichloromethane (6×50 mL), the combined organic layers dried over anhydrous $MgSO_4$, and the solvent concentrated *in vacuo* to yield **L1** as a brown oil which crystallised on standing (1.63 g, 49%). An equivalent procedure can be used to generate **HL2.** Characterisation data were consistent with the commercial material and these solids were used without further purification.

3. Additional Figures
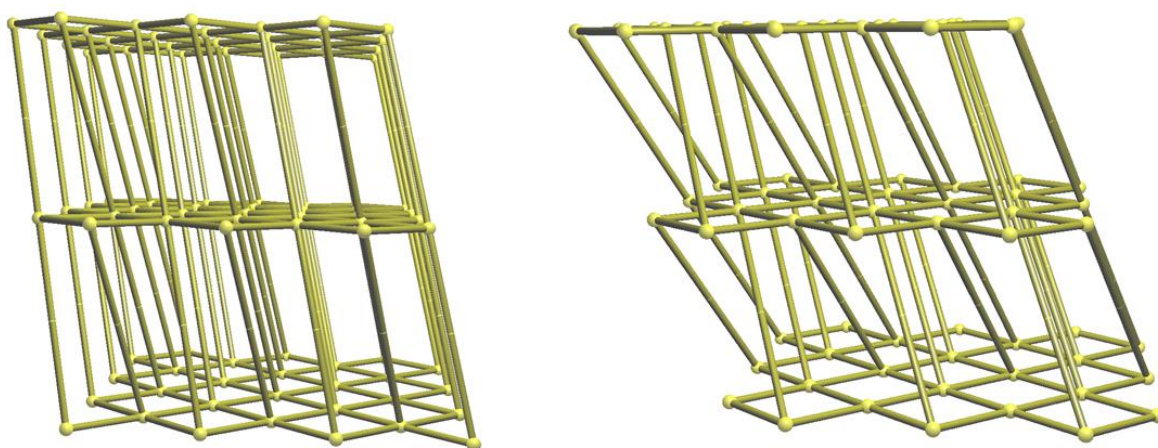
Figure S1 Simplified representations of the **rob** (complex **1**, left) and **mab** (complex **2**, right) topologies.
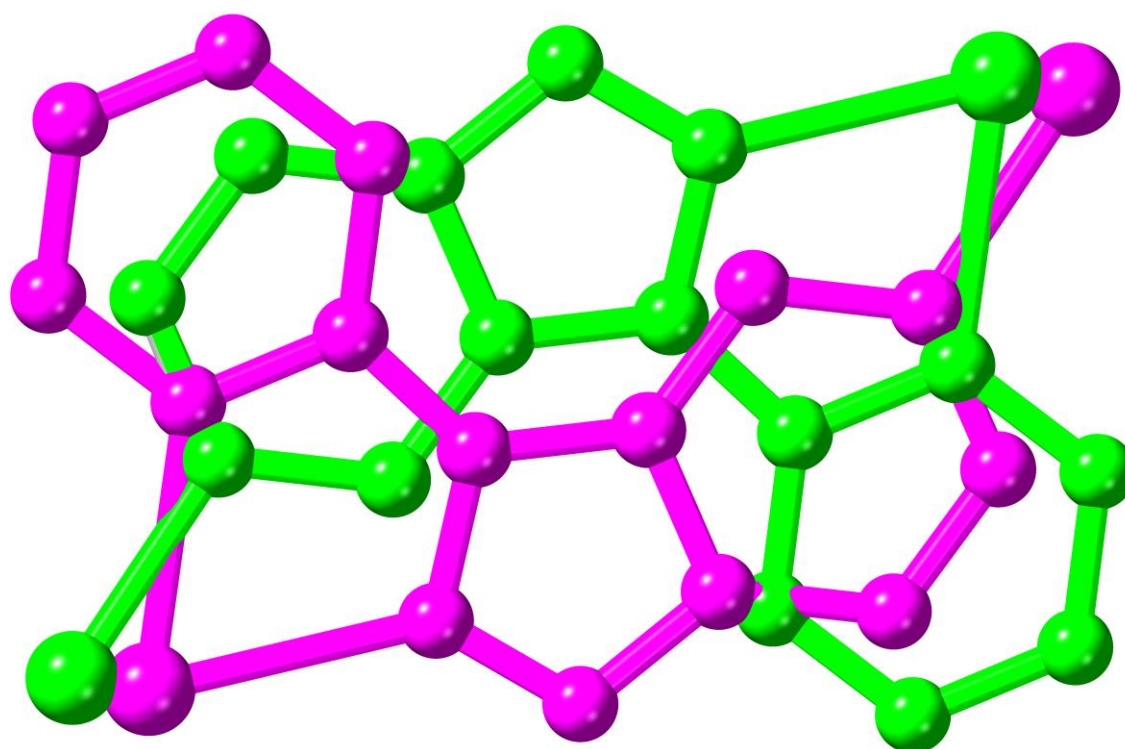
Figure S2 Representation of the disorder mode across the inversion centre which overlaps with the bridging **L5** ligand in complex **5β**. The two disordered contributors are coloured separately, and hydrogen atoms are omitted for clarity.

4. UV-Visible and Fluorescence Spectroscopy
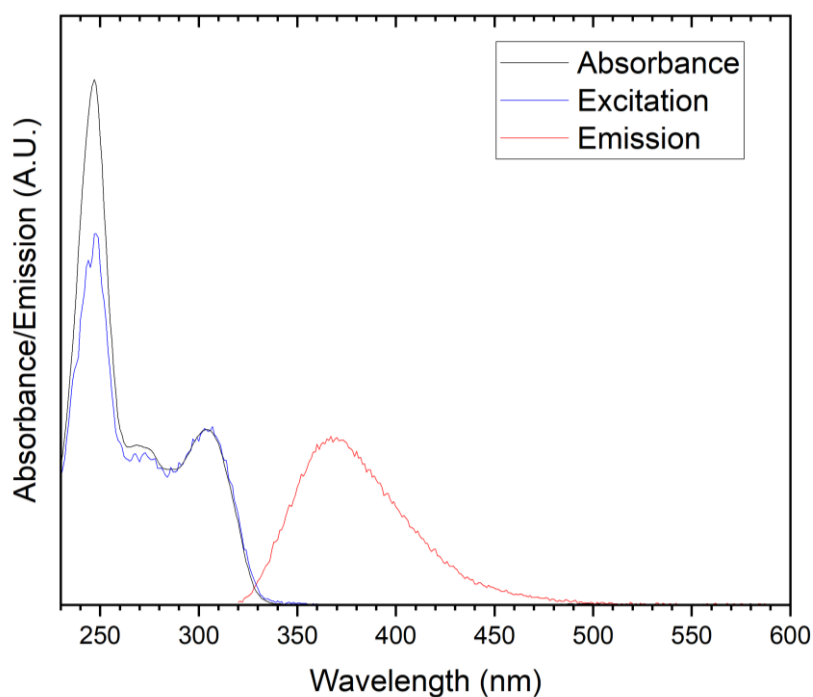
Figure S3 Overlaid absorption, emission (λ_{ex} = 310 nm) and excitation (λ_{em} = 366nm) spectra for **L3** measured in acetonitrile at 10.7 μM.
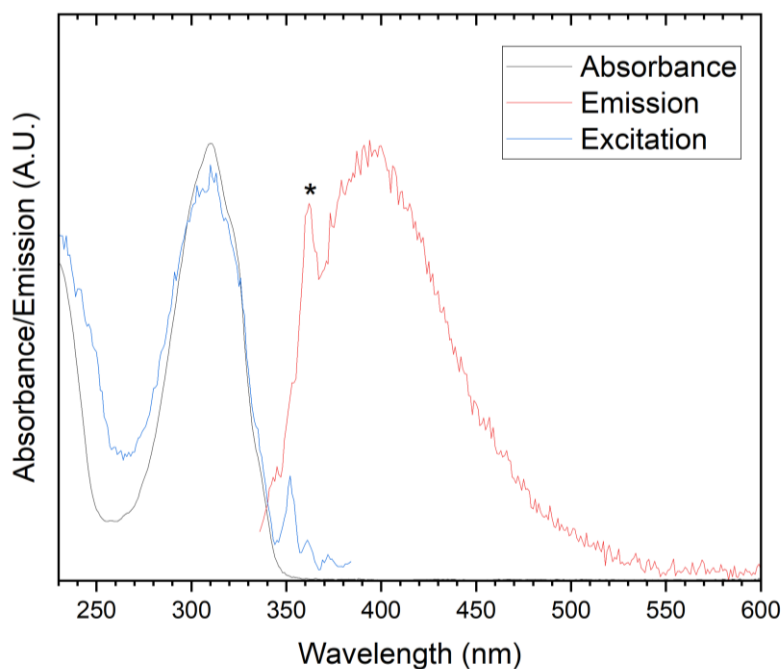
Figure S4 Overlaid absorption, emission (λ_{ex} = 326 nm) and excitation (λ_{em} = 394nm) spectra for **L4** measured in acetonitrile at 10.8 μM. * represents a Raman band from the solvent, visible due to the low emission intensity for this compound.
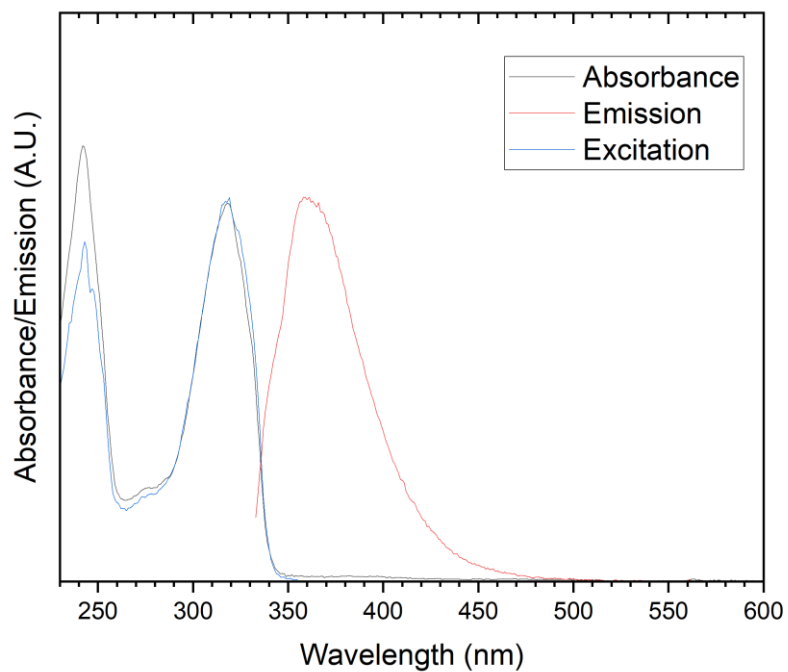
Figure S5 Overlaid absorption, emission (λ_{ex} = 328 nm) and excitation (λ_{em} = 360nm) spectra for **L5** measured in acetonitrile at 10.2 μM.
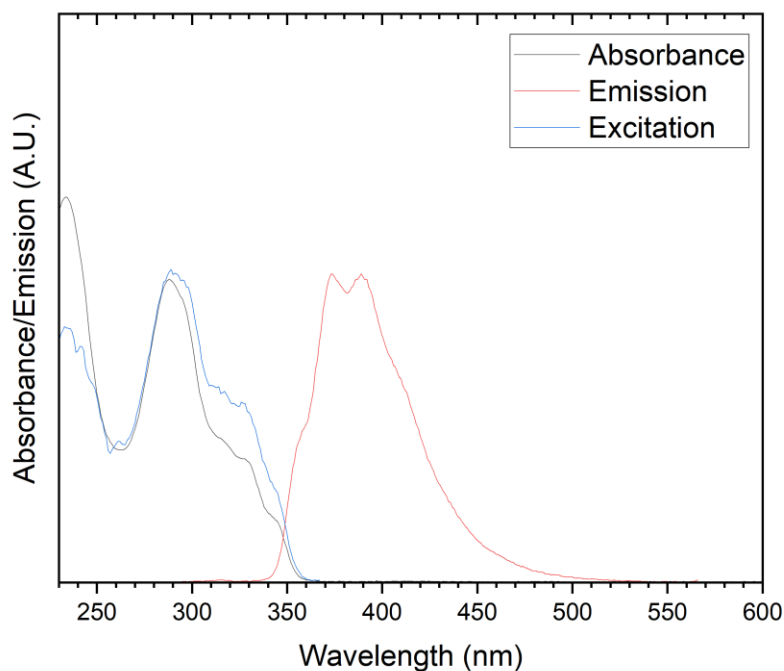
Figure S6 Overlaid absorption, emission (λ_{ex} = 287 nm) and excitation (λ_{em} = 375 nm) spectra for **L6** measured in acetonitrile at 10.5 μM.
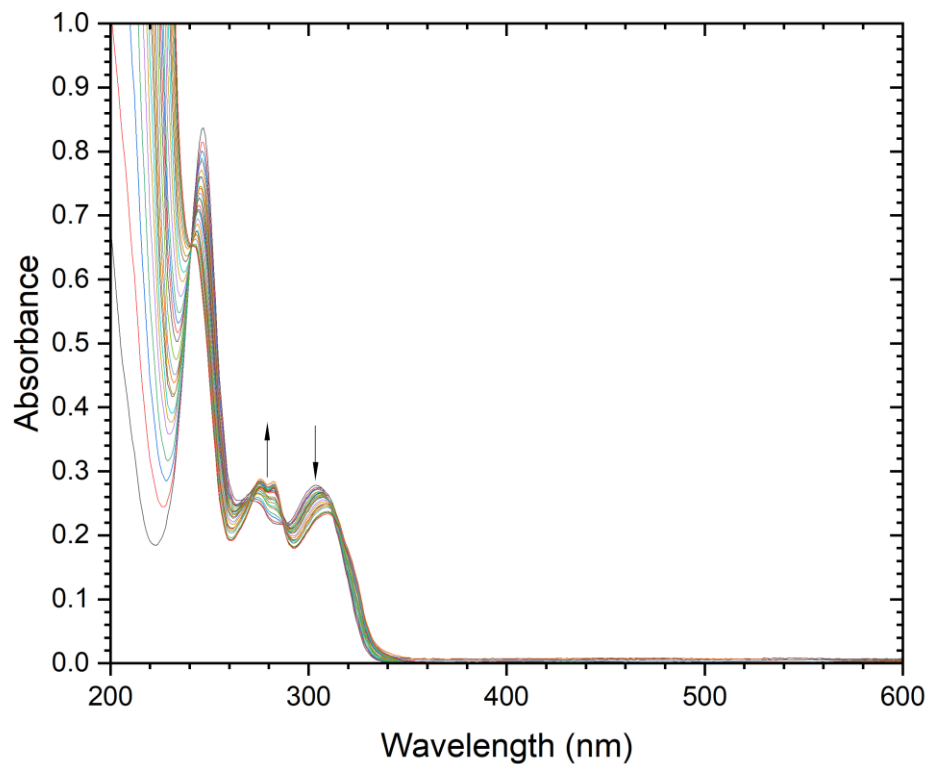
Figure S7 Overlaid UV/Visible absorption spectra for the addition of zinc nitrate hexahydrate aliquots (0 – 70 eq.) to **L3** (27 μM) in MeCN.
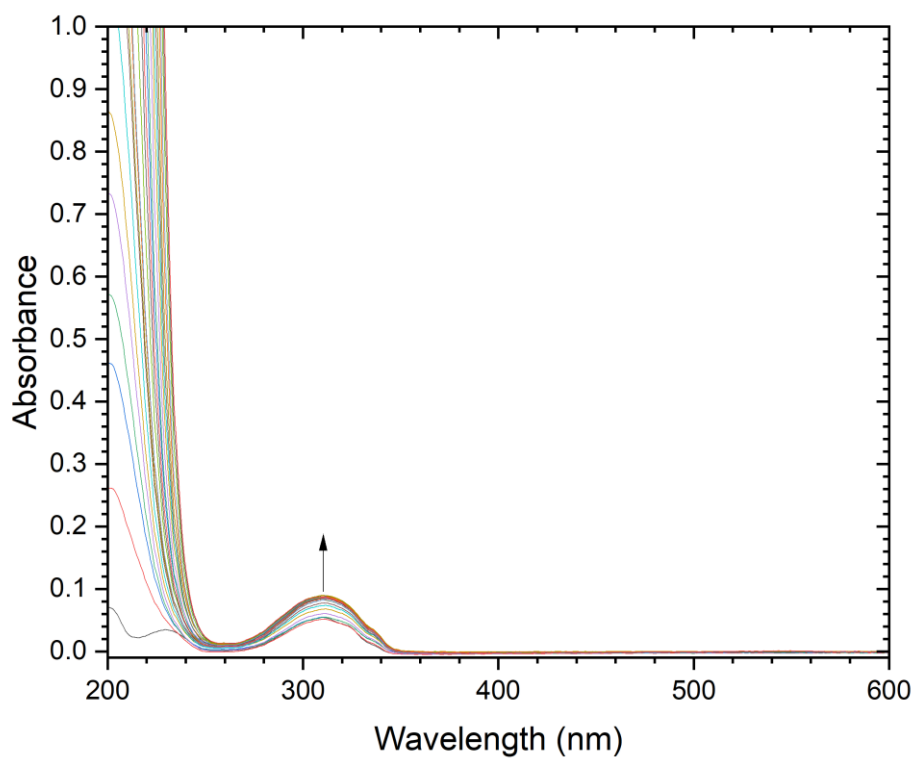
Figure S8 Overlaid UV/Visible absorption spectra for the addition of zinc nitrate hexahydrate aliquots (0 – 46 eq.) to **L4** (14 μM) in MeCN.
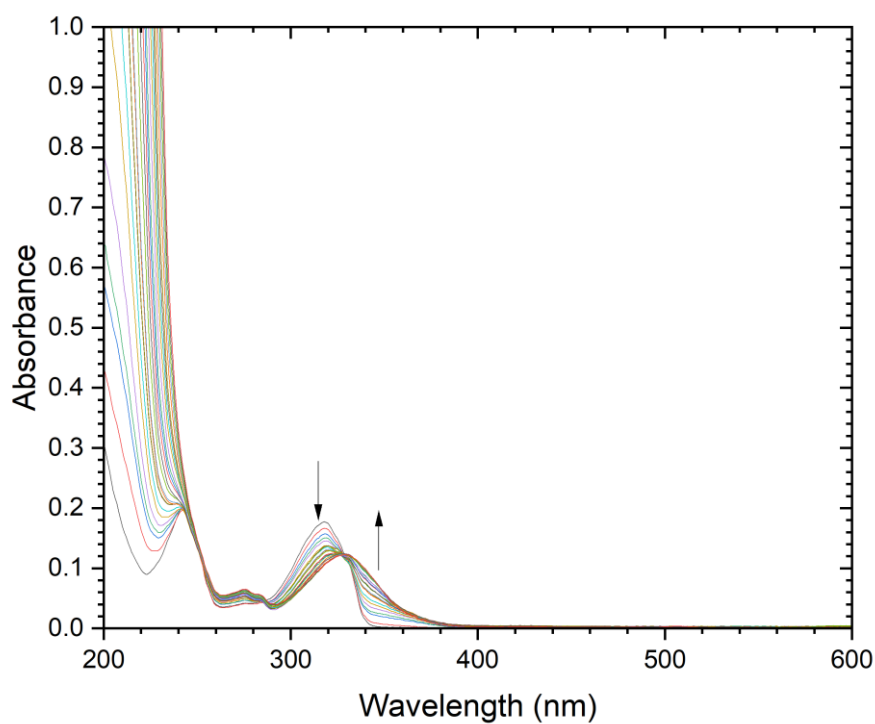
Figure S9 Overlaid UV/Visible absorption spectra for the addition of zinc nitrate hexahydrate aliquots (0 – 86 eq.) to **L5** (13 μM) in MeCN.
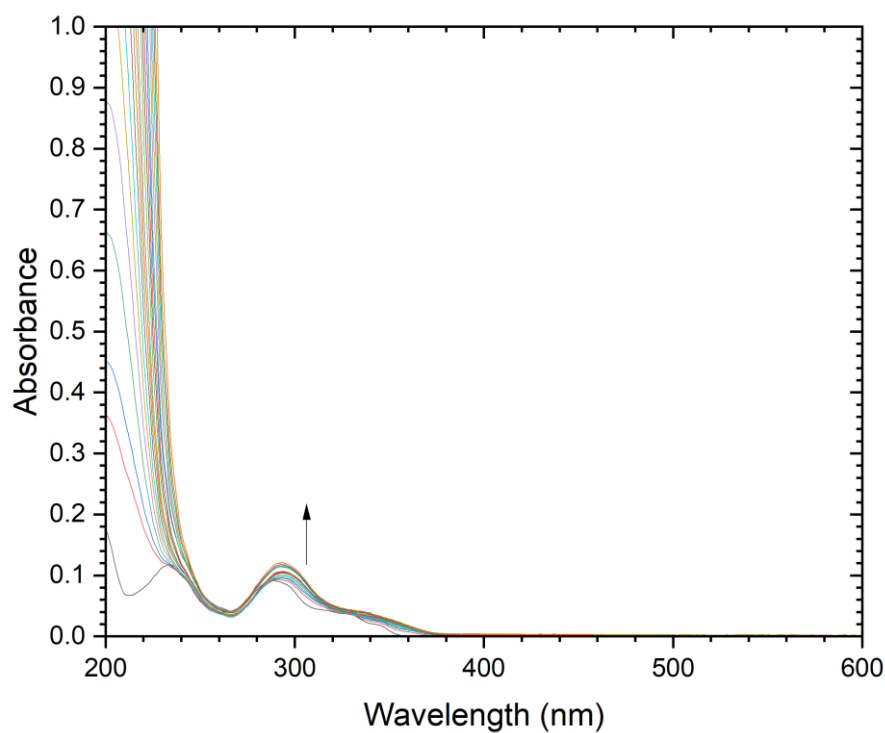
Figure S10 Overlaid UV/Visible absorption spectra for the addition of zinc nitrate hexahydrate aliquots (0 – 34 eq.) to **L6** (13 μM) in MeCN.
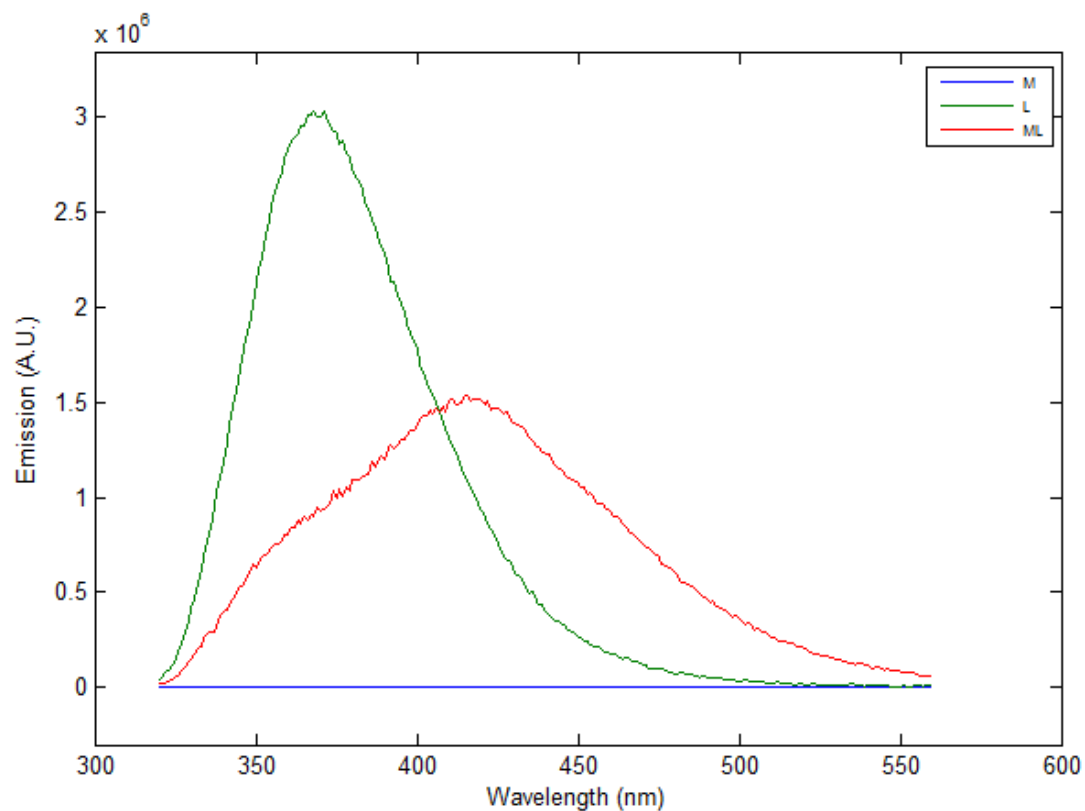
Figure S11 Simulated emission spectra calculated from the global fit for the titration of zinc(II) with **L3**
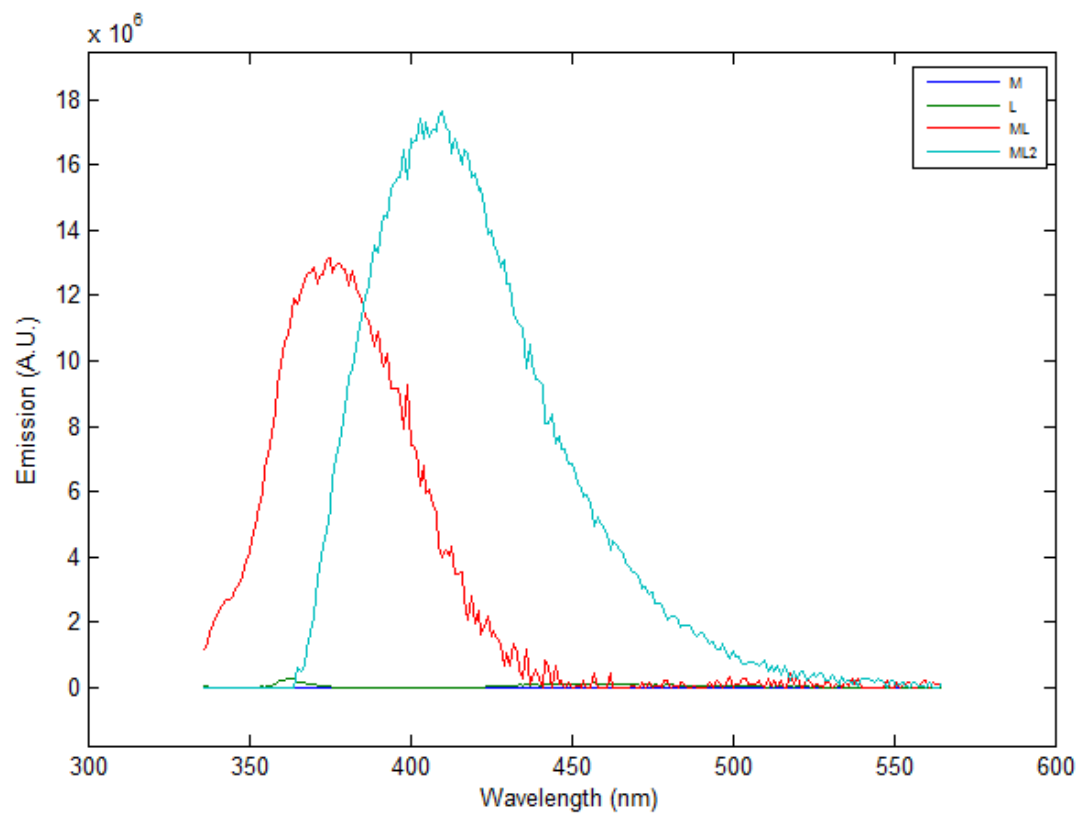
Figure S12 Simulated emission spectra calculated from the global fit for the titration of zinc(II) with **L4**
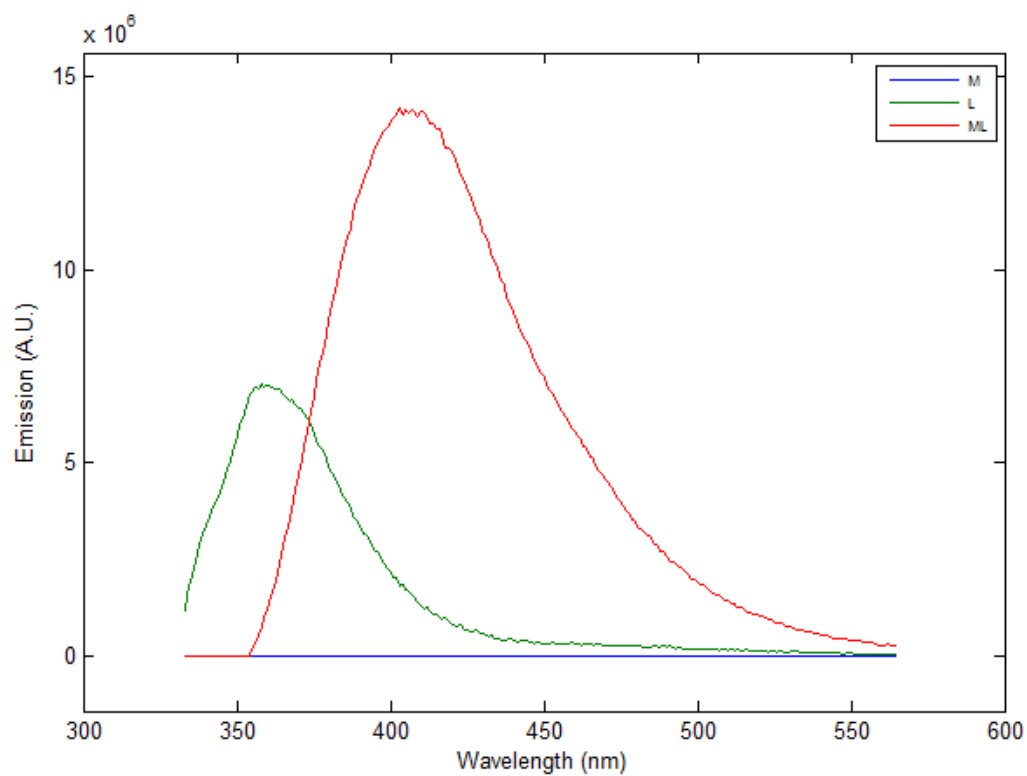
Figure S13 Simulated emission spectra calculated from the global fit for the titration of zinc(II) with **L5**
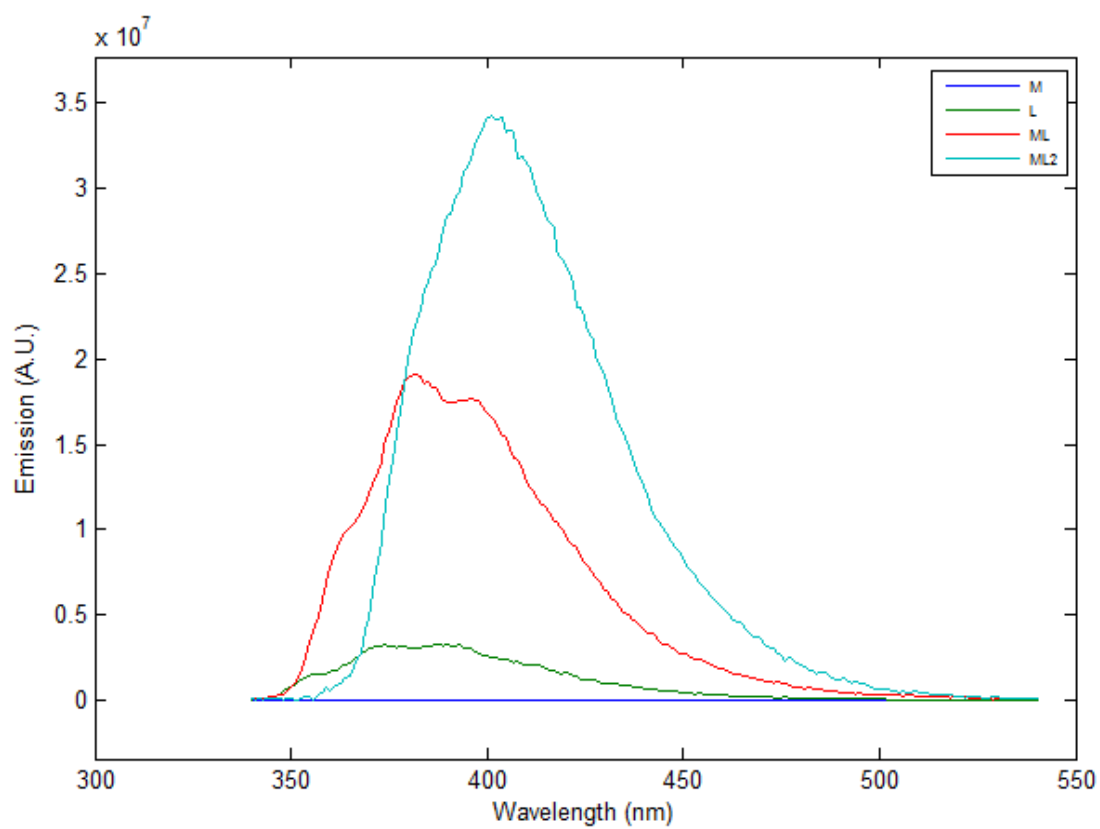
Figure S14 Simulated emission spectra calculated from the global fit for the titration of zinc(II) with **L6**

5. Thermogravimetric Analysis
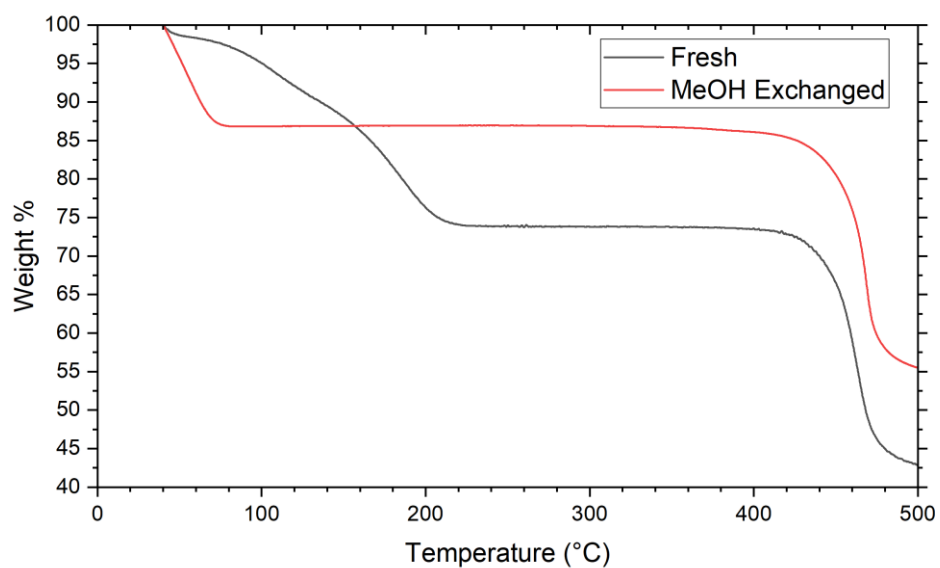
Figure S15 Thermogravimetric analysis plot for complex **1** showing the freshly isolated material (black) and following exchange with methanol (red)
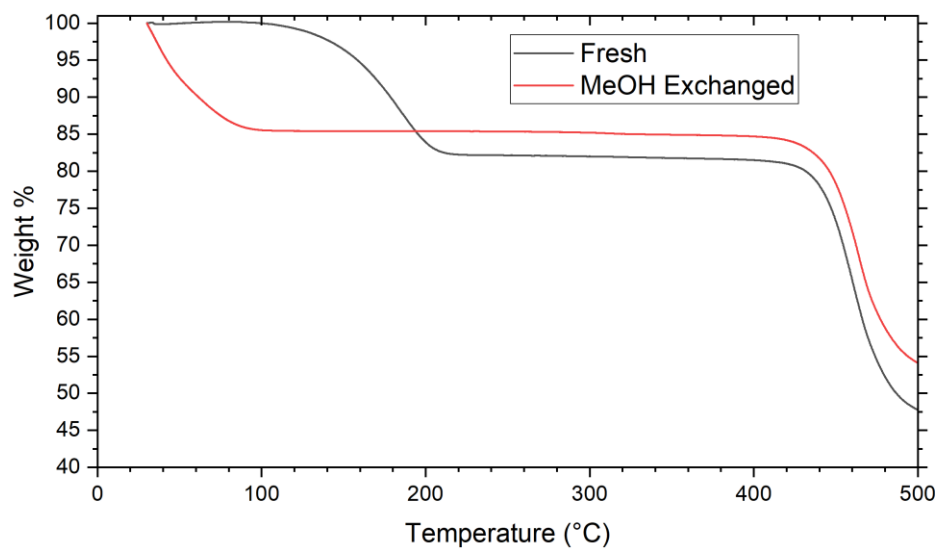
Figure S16 Thermogravimetric analysis plot for complex **2** showing the freshly isolated material (black) and following exchange with methanol (red)

6. Gas Adsorption Figures and Data
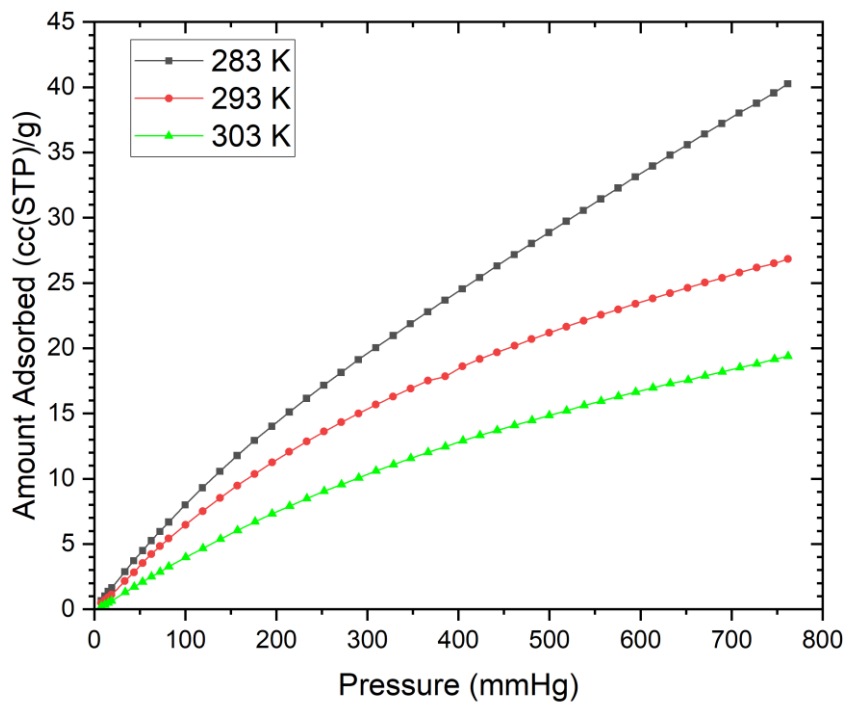
Figure S17 CO_2 adsorption isotherms at 283, 293 and 303 K for compound **1**
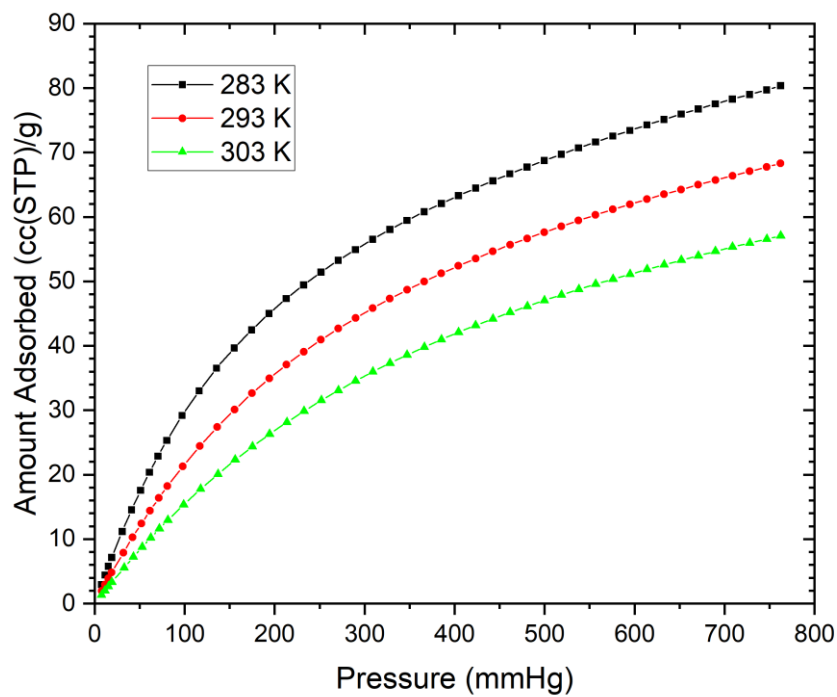
Figure S18 CO_2 adsorption isotherms at 283, 293 and 303 K for compound **2**
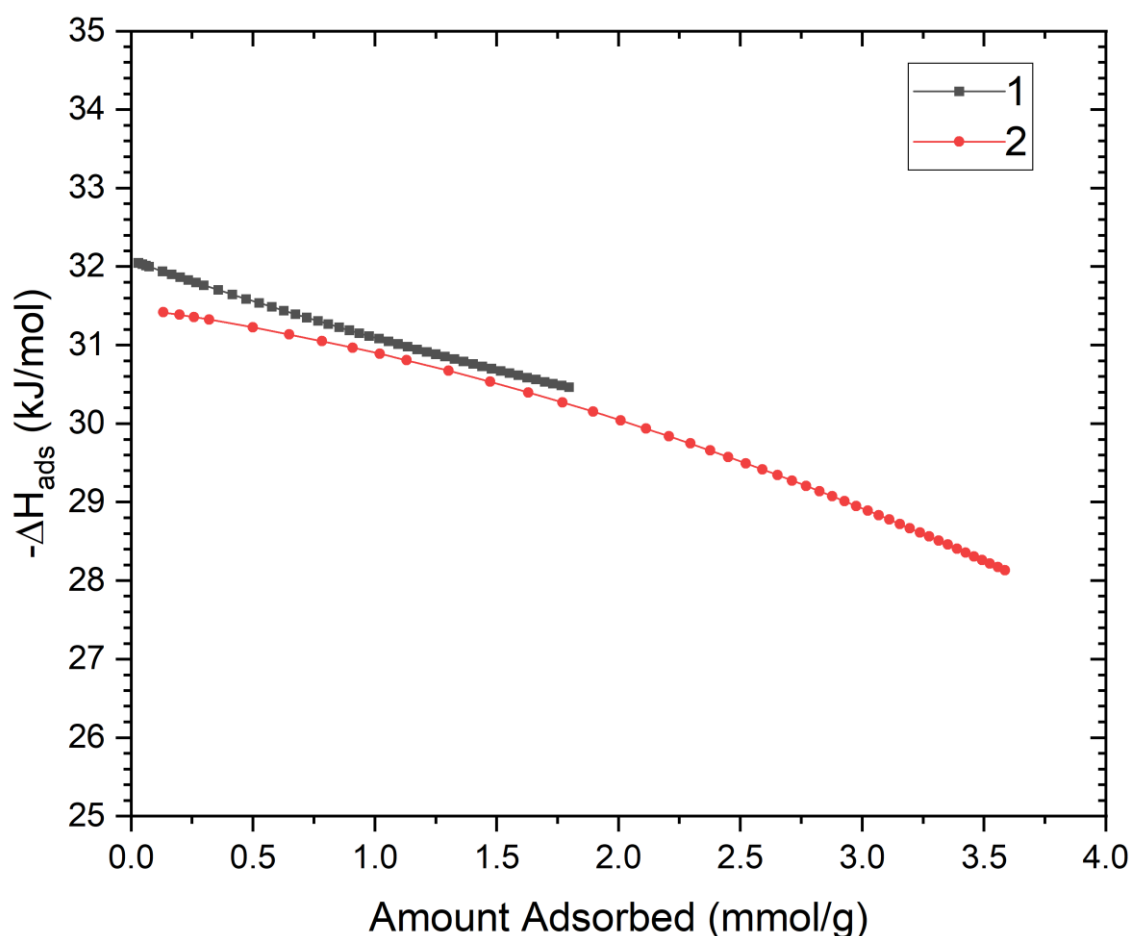
Figure S19 Calculated CO_2 adsorption enthalpy for compounds **1** (black) and **2** (red) across their measured (283 K) loading ranges.

Enthalpy of Adsorption Calculations

The isosteric heat of adsorption for CO_2 in complexes **1** and **2** was estimated using a least-squares fit of a virial thermal adsorption equation which models $\ln(P)$ as a function of gas loading.[S10] The fitted function has the form $\ln(P) = \{\ln(N) + (a_0 + a_1N + a_2N^2\ldots)/T + b\}$, where N represents the surface excess adsorption (mmol) at temperature T and a_0, a_1 and a_2 are coefficients determined through least-squares fitting. The original parameter set of 5 parameters was sequentially reduced to maximise the data:parameter ratio. The enthalpy of adsorption is then given by the relation $Q(N) = -R(a_0 + a_1N + a_2N^2\ldots)$. Optimised coefficients and parameters are given below.

Compound	1	2
Temperatures (K)	283, 293, 303	283, 293, 303
a_0	-3858.28	-3786.35
a_1	130.4479	52.7522
a_2	-12.3849	16.6223
B	17.04772	15.33453
R^2	0.9953	0.9997
Datapoints fitted	138	138
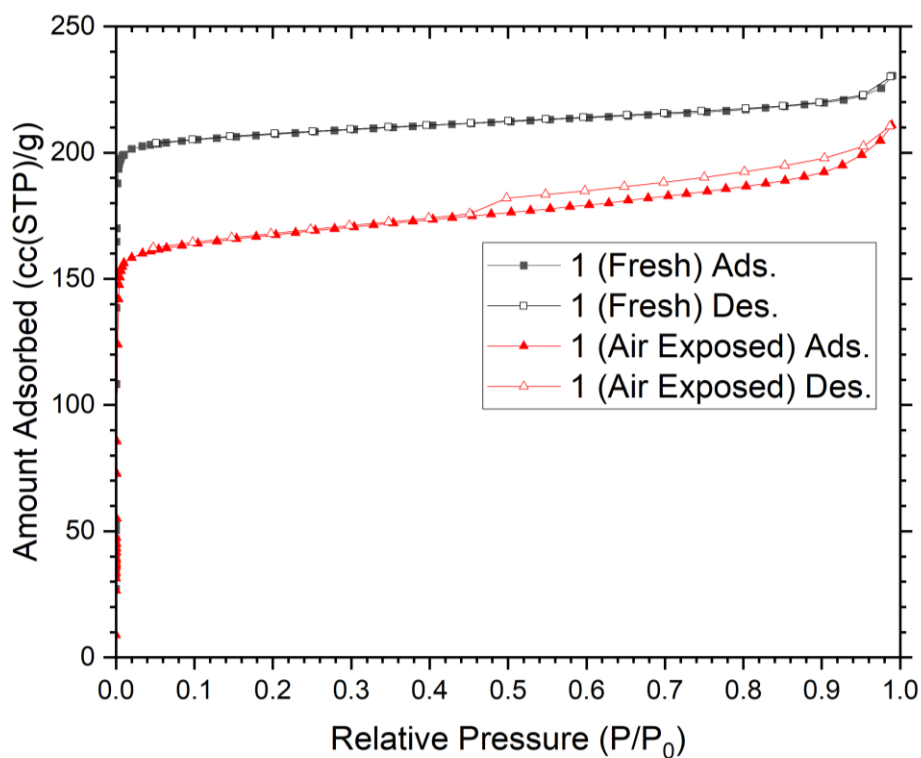
Figure S20 Comparison of N_2 uptake at 77 K for complex **1** before (black) and after exposure to air (red)
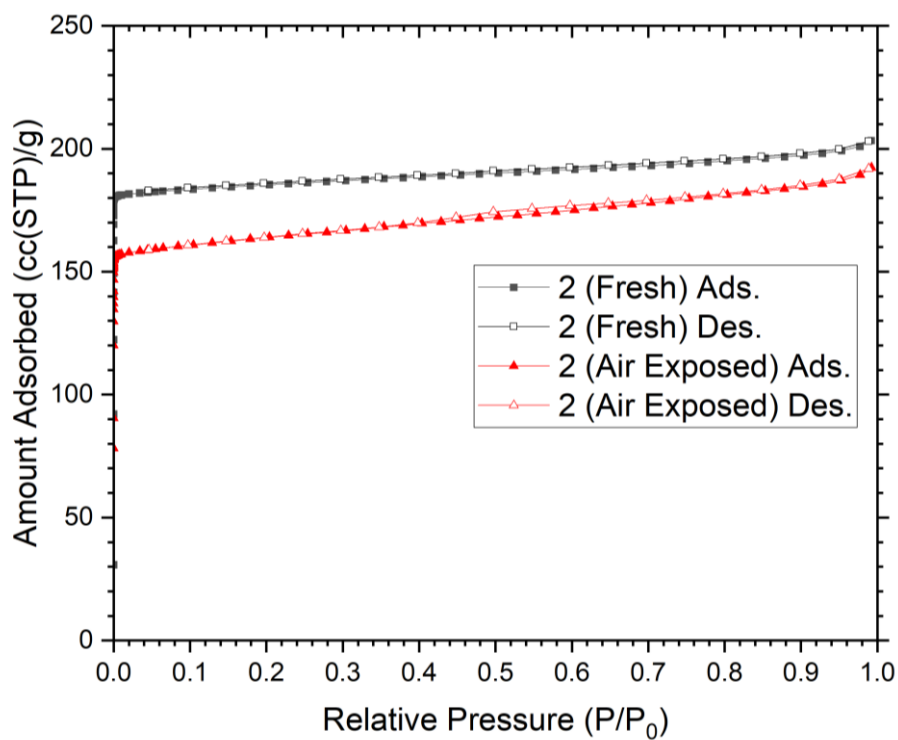
Figure S21 Comparison of N_2 uptake at 77 K for complex **2** before (black) and after exposure to air (red)

BET Surface Area Calculation Parameters

Complex 1	
Fresh Sample	
Slope	4.037 (g^{-1})
Intercept	2.481e-04 (g^{-1})
Correlation Coefficient, r	0.999997
C constant	16275.142
Surface Area	862.491 m^2/g
After Air Exposure	
Slope	5.074 (g^{-1})
Intercept	1.358e-03 (g^{-1})
Correlation Coefficient, r	0.999951
C constant	3736.673
Surface Area	686.156 m^2/g
Complex 2	
Fresh Sample	
Slope	4.441 (g^{-1})
Intercept	7.597e-06 (g^{-1})
Correlation Coefficient, r	1.000000
C constant	584607.151
Surface Area	784.107 m^2/g
After Air Exposure	
Slope	5.132 (g^{-1})
Intercept	1.460e-05 (g^{-1})
Correlation Coefficient, r	1.000000
C constant	351552.546
Surface Area	678.648 m^2/g
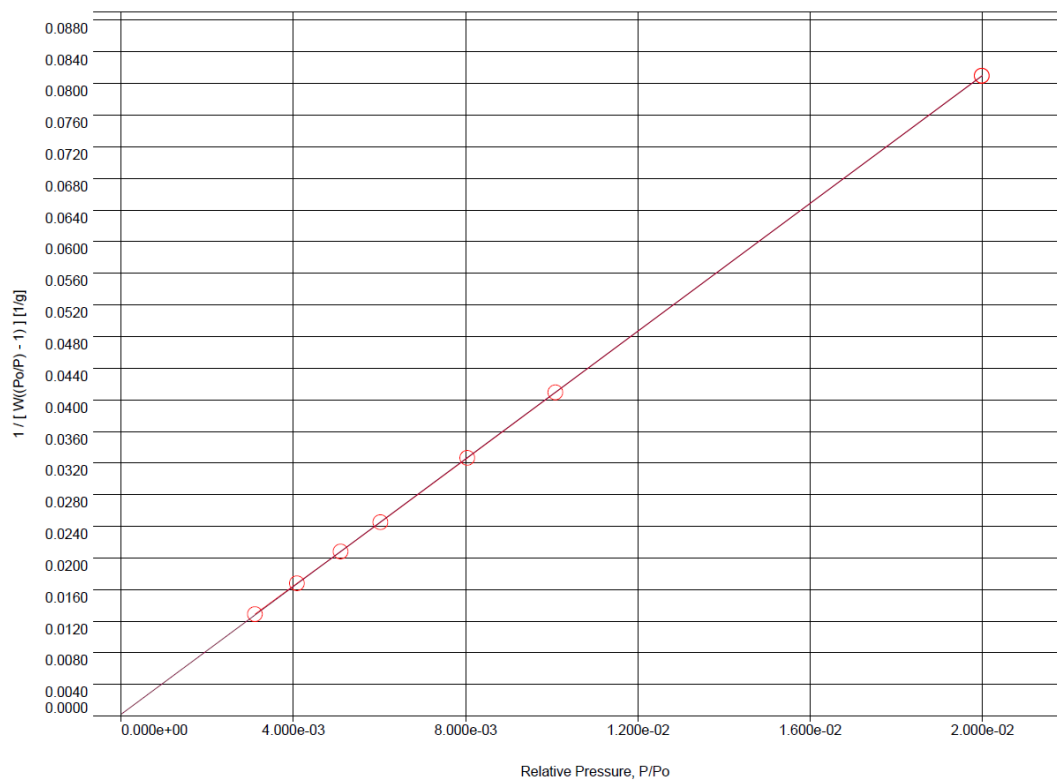
Figure S22 BET fit for complex **1** (fresh)
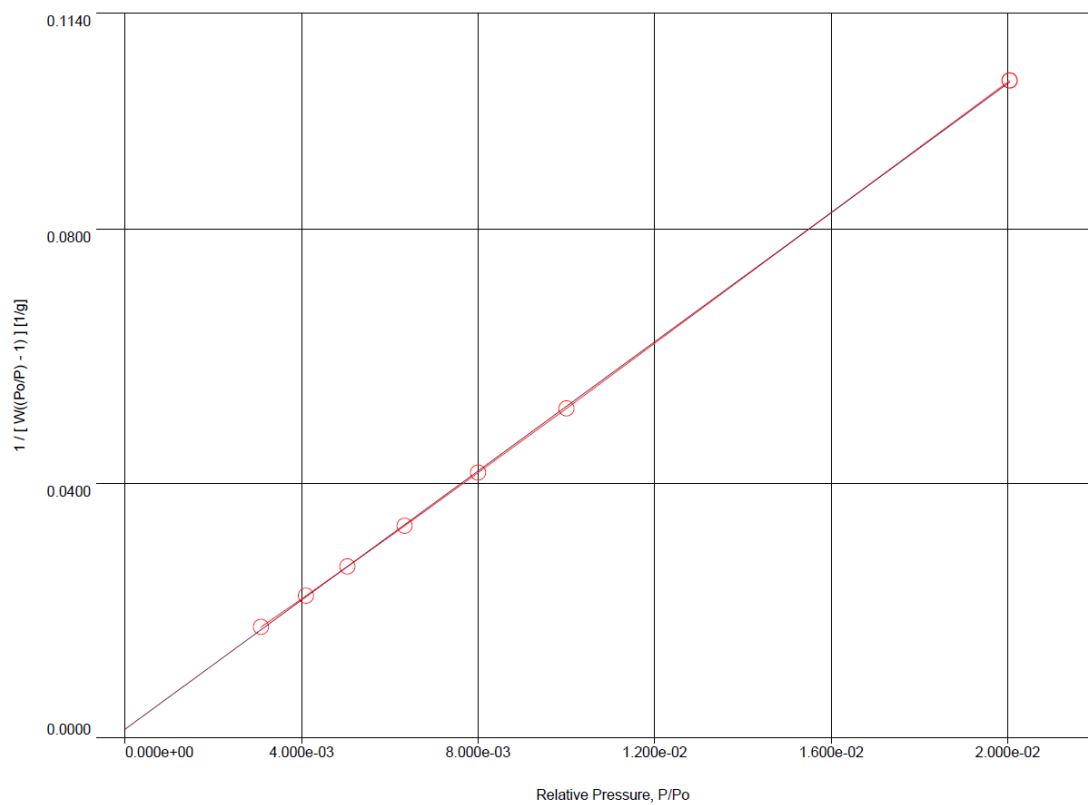
Figure S23 BET fit for complex **1** (air exposed)
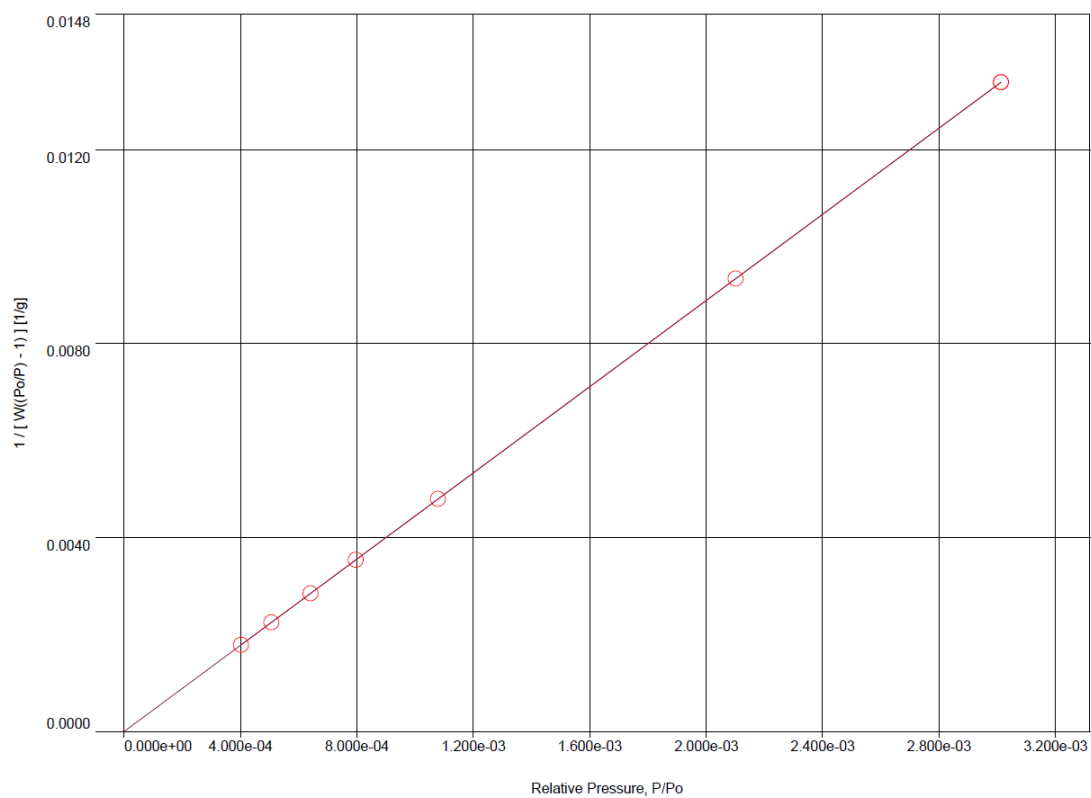
Figure S24 BET fit for complex **2** (fresh)
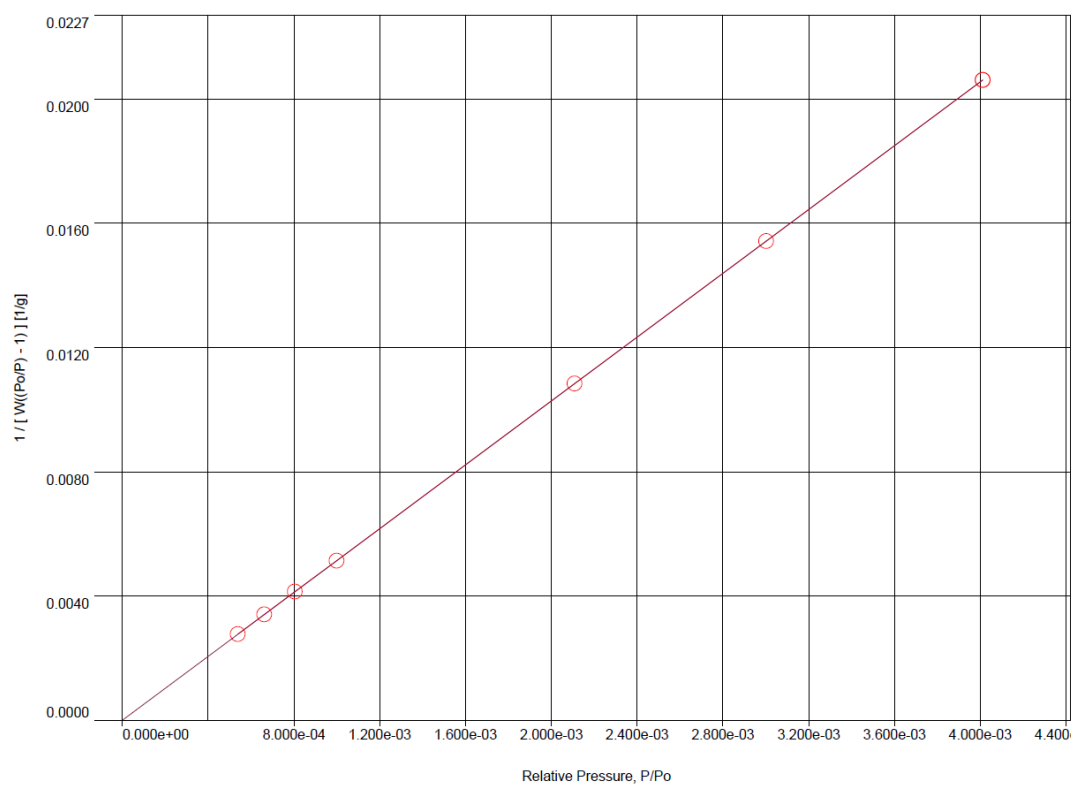
Figure S25 BET fit for complex **2** (air exposed)
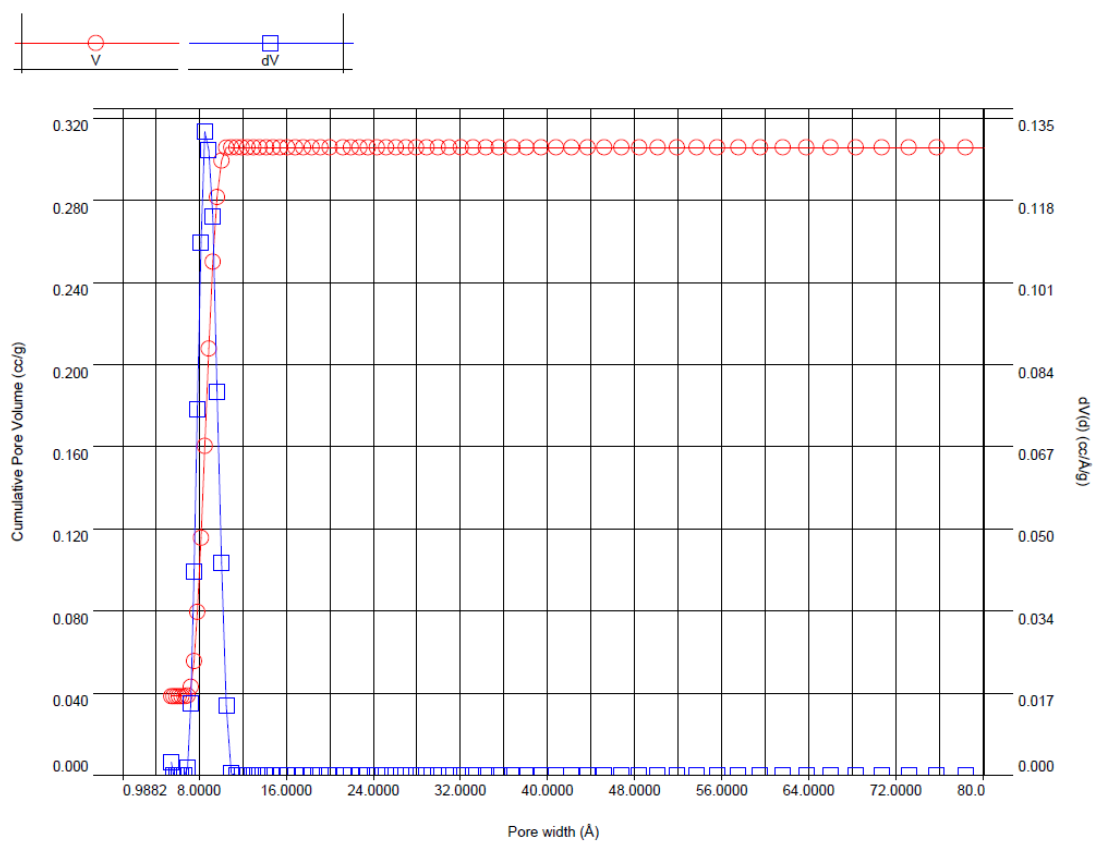
Figure S26 Calculated pore size distribution for complex **1** showing the presence of a single type of micropores of average diameter *ca.* 8.5 Å
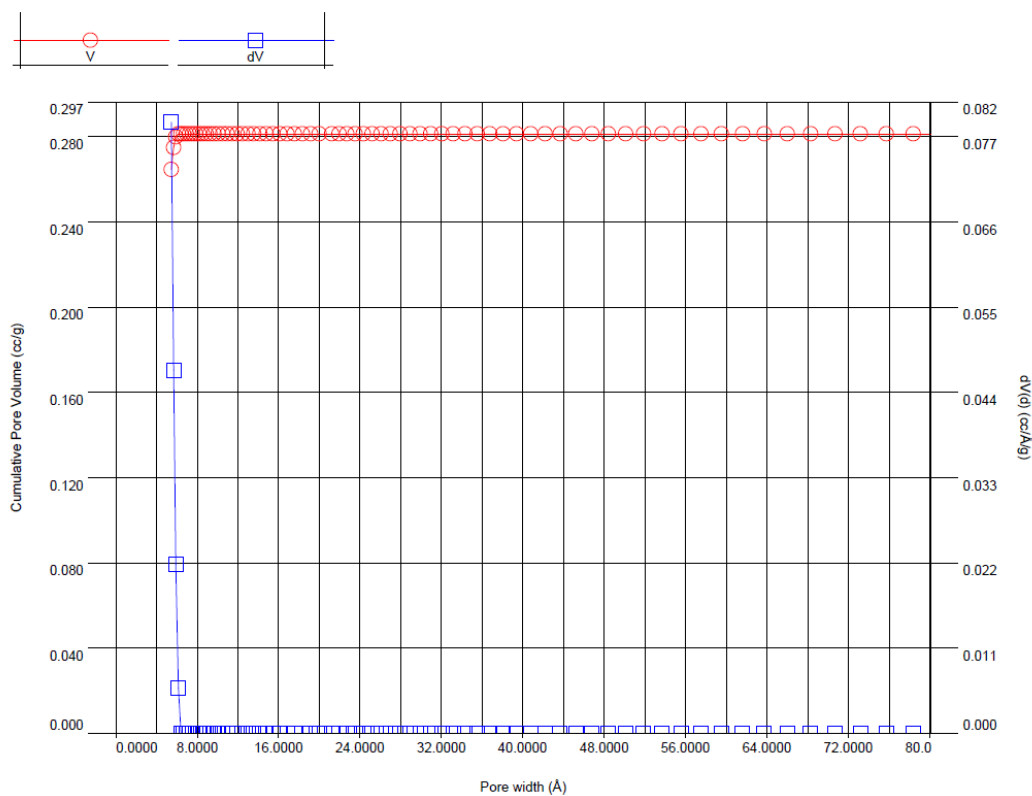

Figure S27 Calculated pore size distribution for complex **2** showing the presence of micropores with average diameter < 5.5 Å.

7. X-ray Powder Diffraction
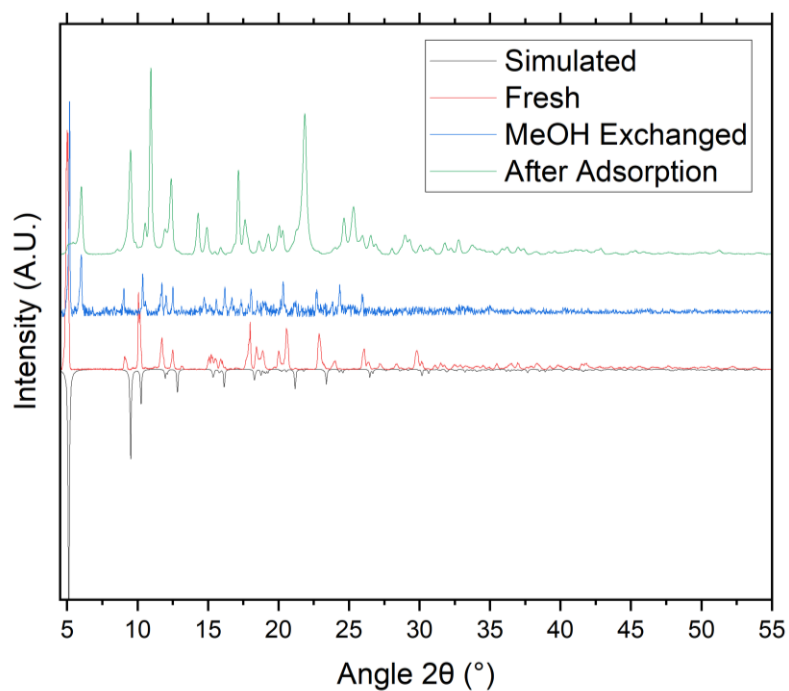
Figure S28 X-ray powder patterns for **1** collected at room temperature, showing the freshly isolated material (red), the compound soaked in methanol (blue), and the material following gas adsorption (green), compared with the simulated pattern based on the (150 K) single crystal data (black).
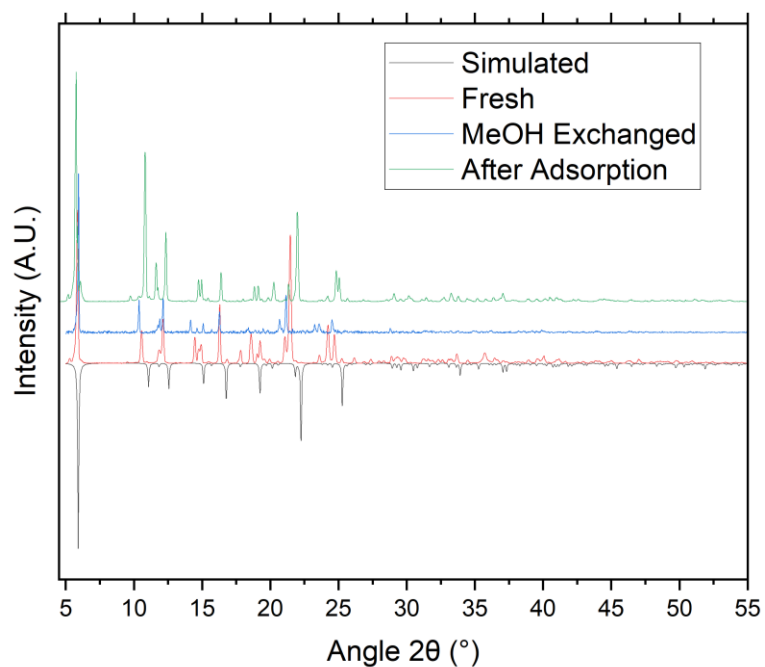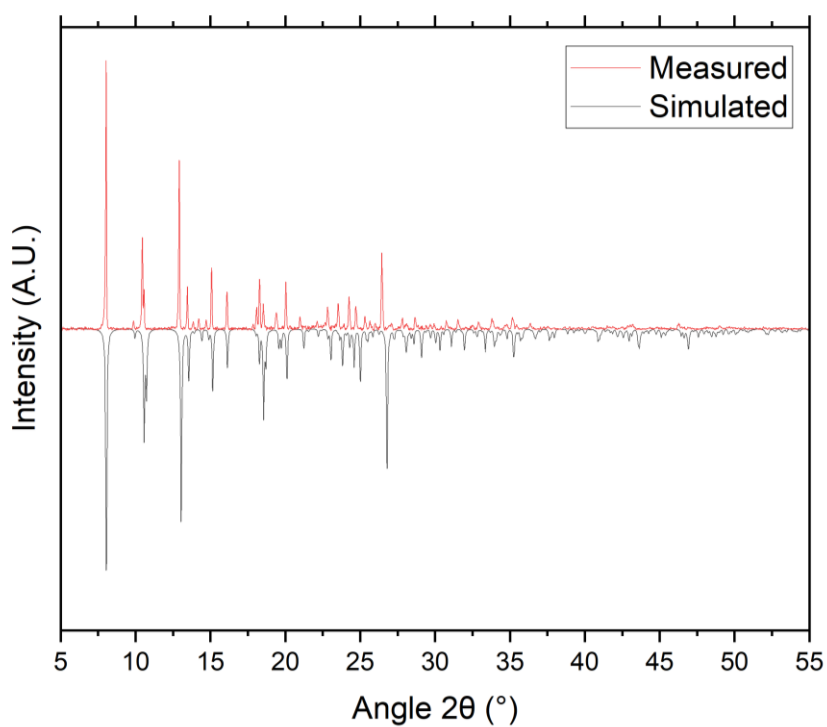

Figure S29 X-ray powder patterns for **2** collected at room temperature, showing the freshly isolated material (red), the compound soaked in methanol (blue), and the material following gas adsorption (green), compared with the simulated pattern based on the (150 K) single crystal data (black)
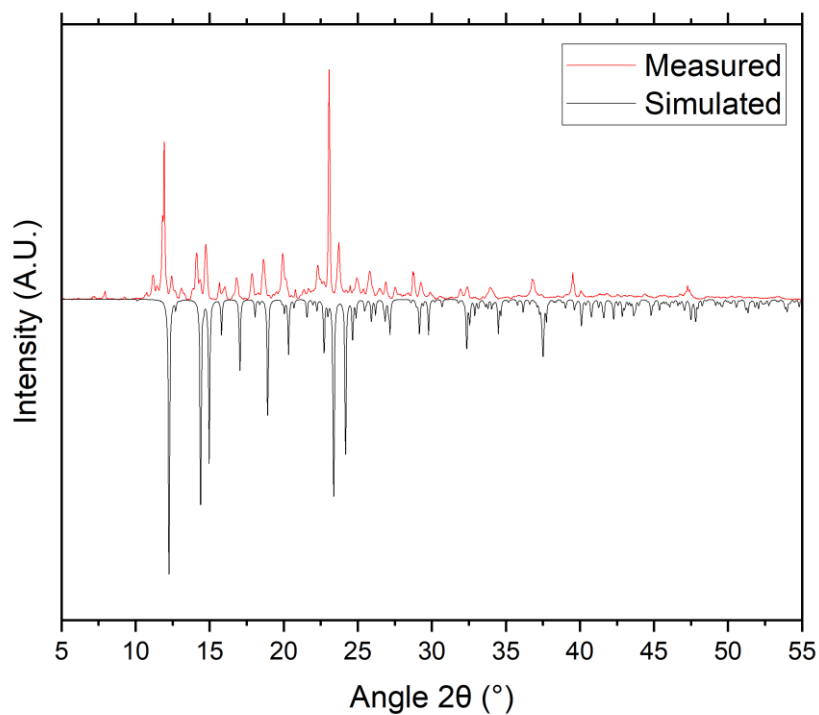
Figure S30 X-ray powder patterns for **3** collected at room temperature (red), compared with the simulated pattern based on the (150 K) single crystal data (black)
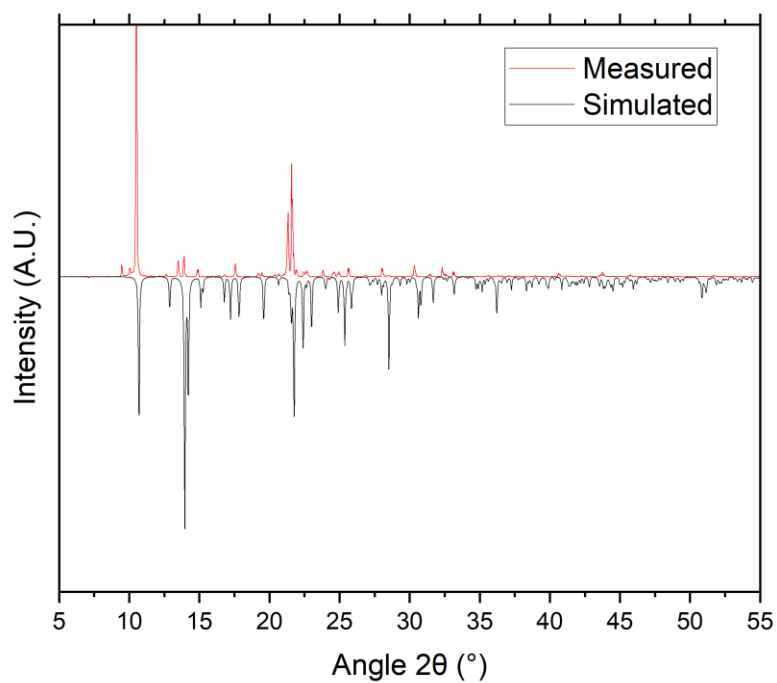
Figure S31 X-ray powder patterns for **4** collected at room temperature (red), compared with the simulated pattern based on the (150 K) single crystal data (black)
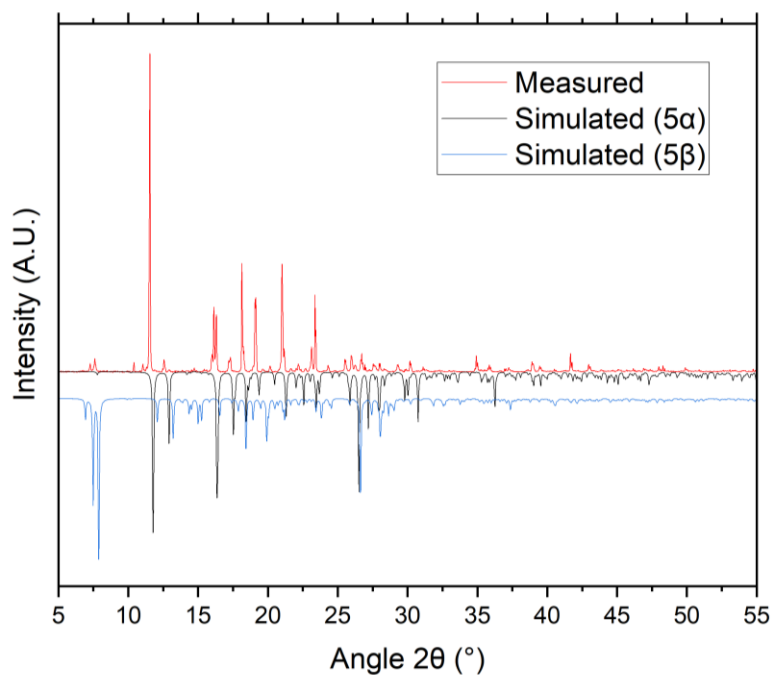
Figure S32 X-ray powder patterns for the crude **5** collected at room temperature (red), compared with the simulated pattern based on the (150 K) single crystal datasets for **5α** (black) and **5β** (blue), with the diagnostic peaks at 7-8 ° indicating the presence of a small amount of **5β**

Figure S33 X-ray powder patterns for **6** collected at room temperature (red), compared with the simulated pattern based on the (150 K) single crystal data (black)

8. NMR Spectroscopy
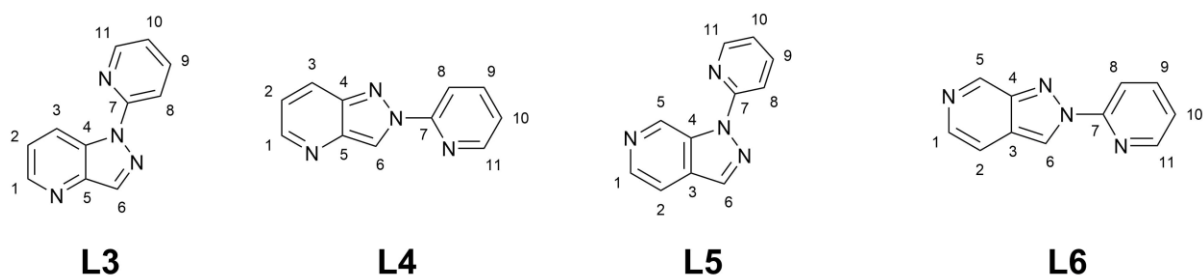
Figure S34 ^{1}H and ^{13}C NMR numbering scheme for ligands **L3 – L6**
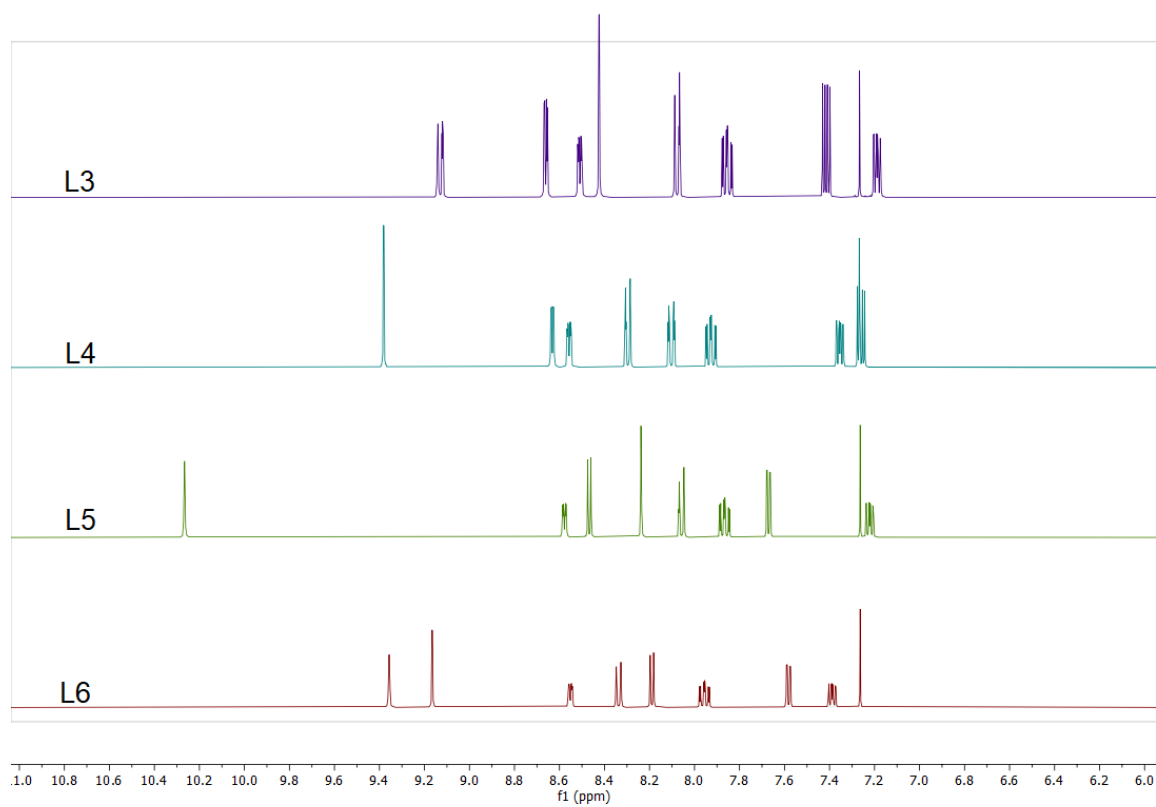
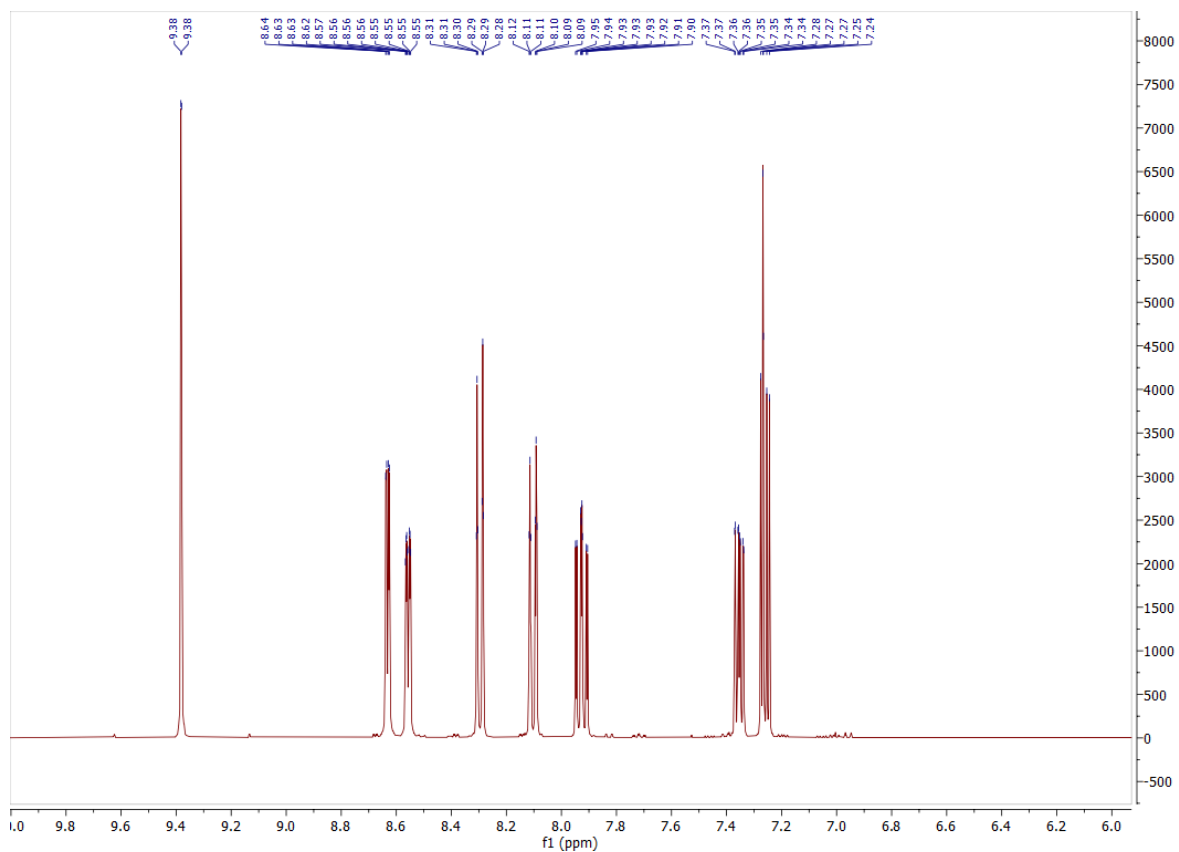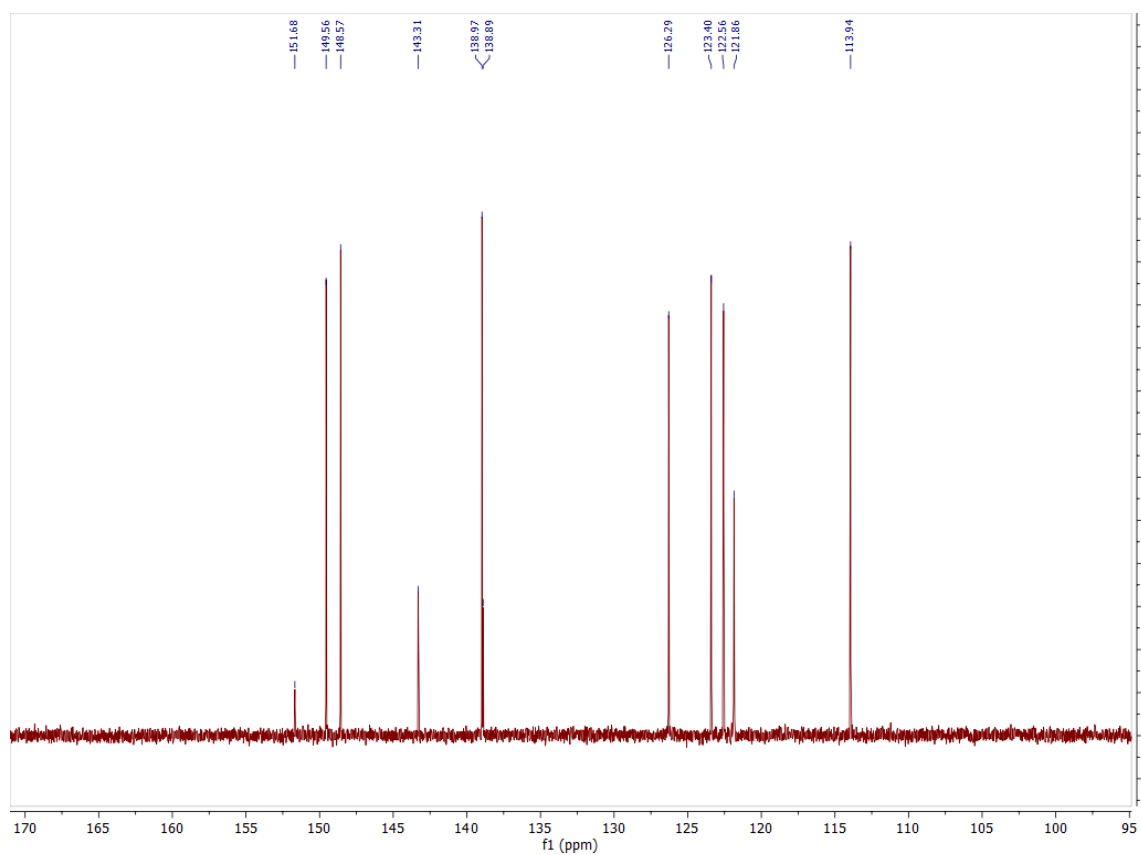**Figure S35** Overlay of ^{1}H NMR spectra for **L3 – L6**
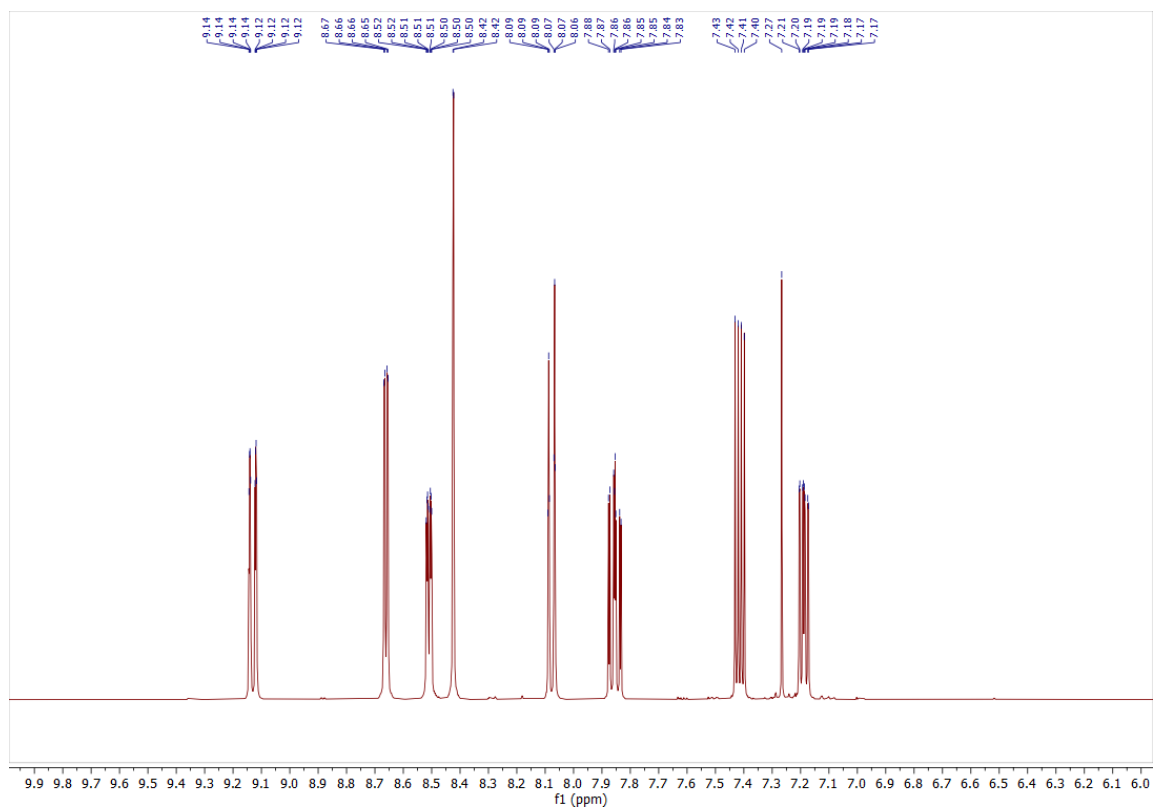
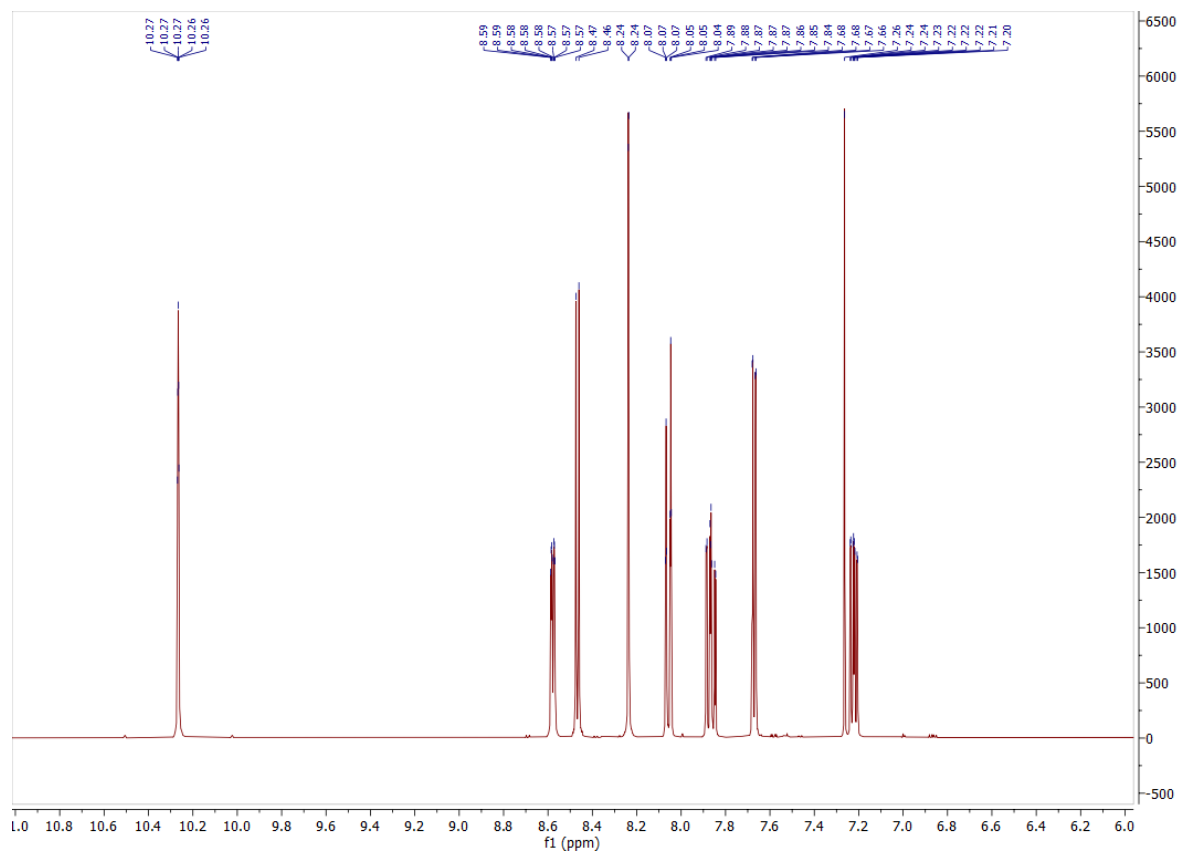**Figure S36** ^{1}H NMR spectrum (CDCl$_3$, 400 MHz) for **L3**
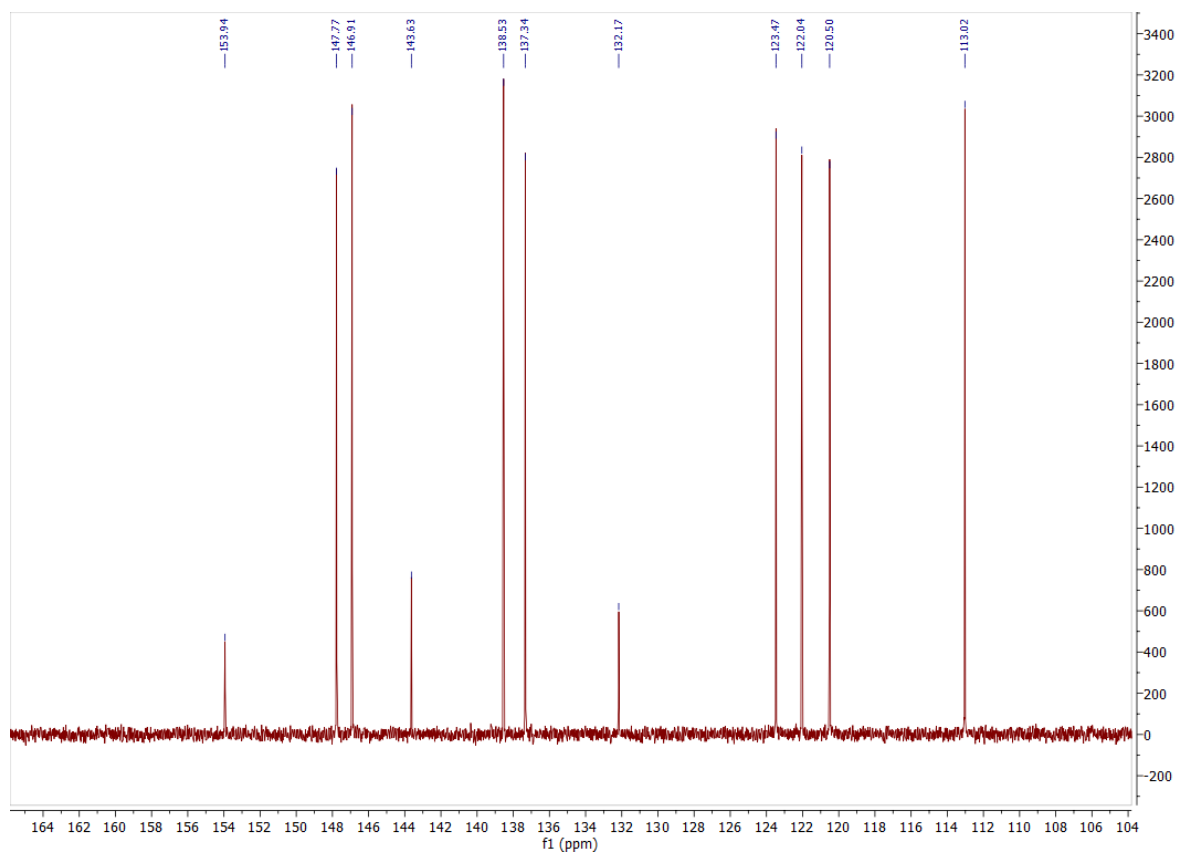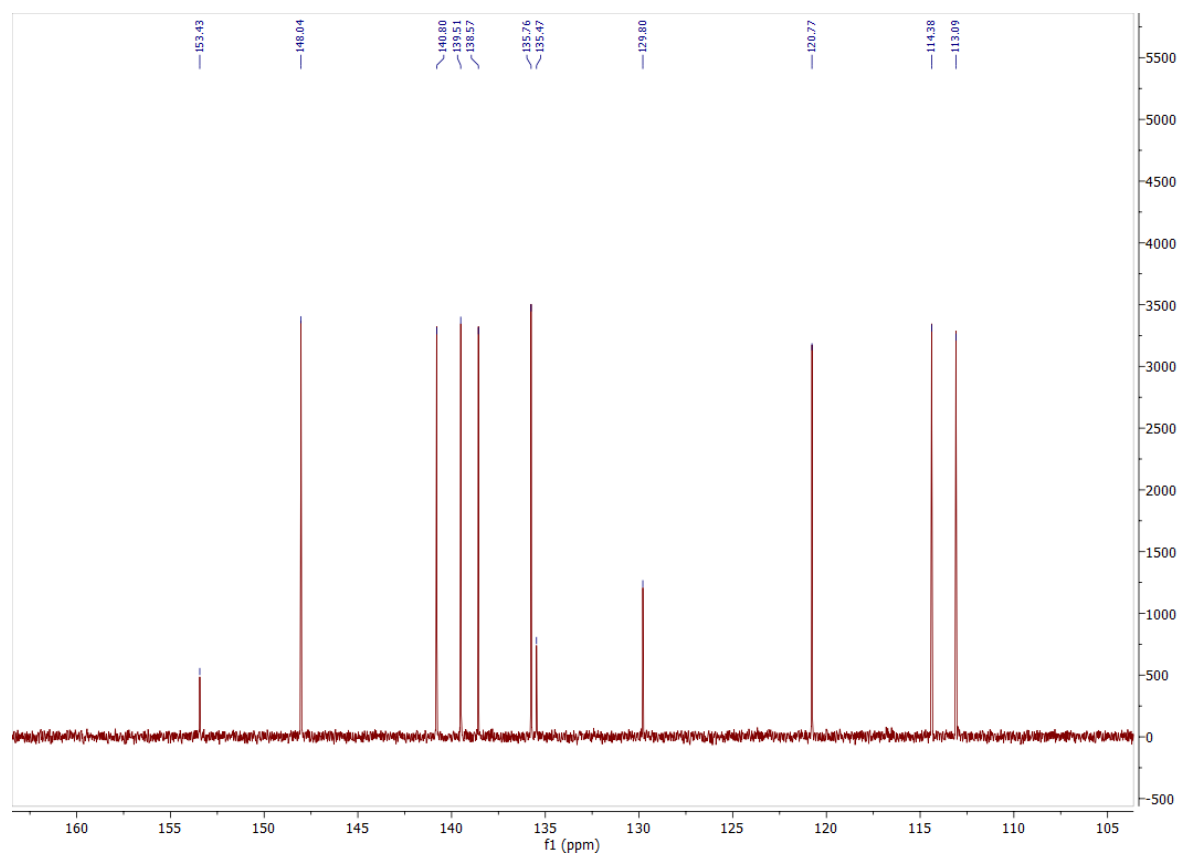

Figure S37 ^{13}C NMR (CDCl$_3$, 101 MHz) for **L3**
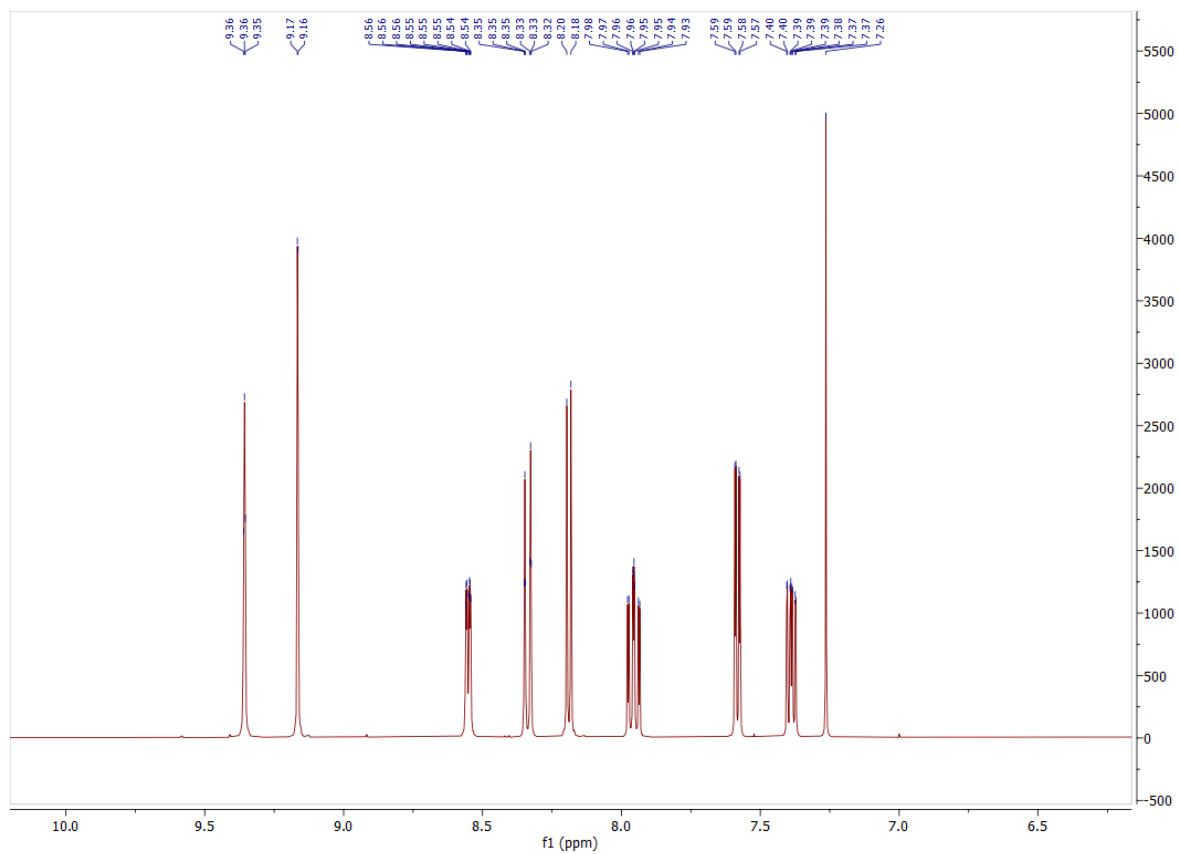
Figure S38 ^{1}H NMR spectrum (CDCl$_3$, 400 MHz) for **L4**
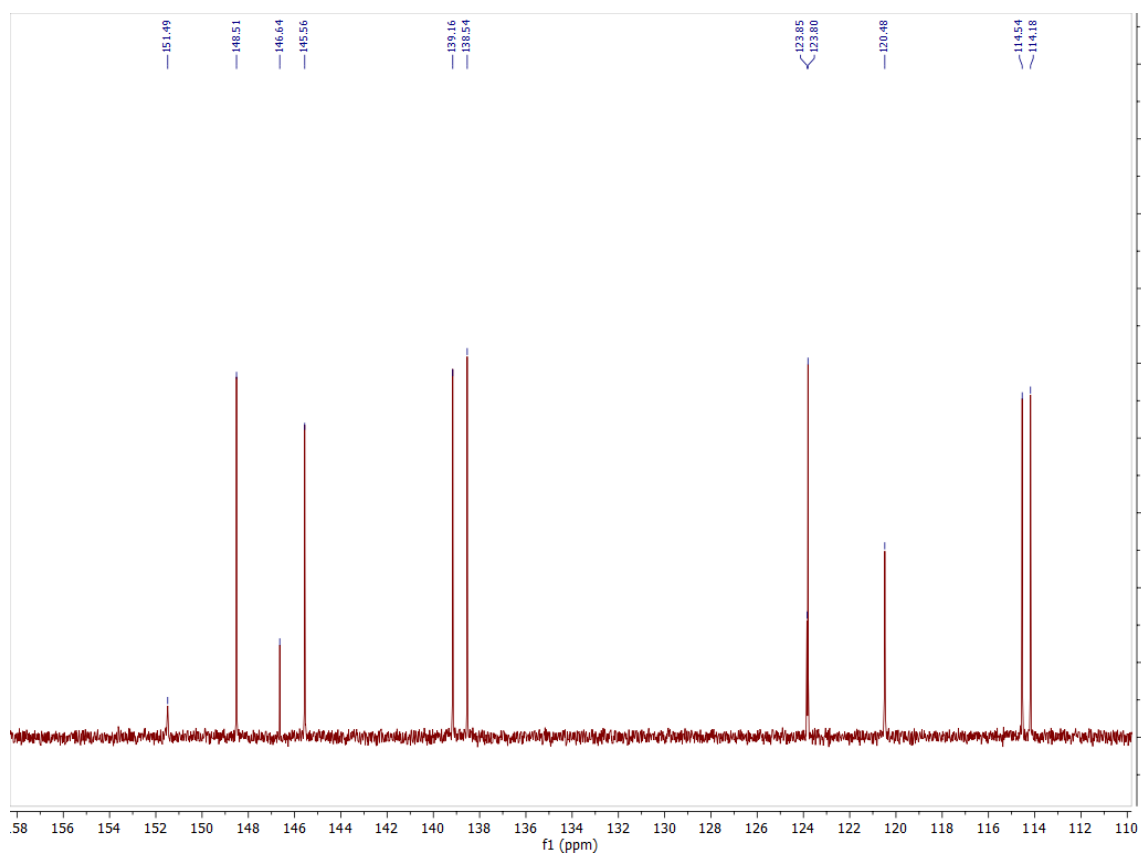

Figure S39 ^{13}C NMR spectrum (101 MHz, CDCl$_3$) for **L4**

Figure S40 ^{1}H NMR spectrum (400 MHz, CDCl$_3$) for **L5**

Figure S41 ^{13}C NMR spectrum (CDCl$_3$, 101 MHz) for **L5**

Figure S42 ^{1}H NMR spectrum (CDCl$_3$, 400 MHz) for **L6**

Figure S43 ^{13}C NMR spectrum (101 MHz, CDCl$_3$) for **L6**

9. References

S1. *ReactLab Equilibria*, Jplus Consulting Ltd., Freemantle, Australia, 2018

S2. *Bruker APEX-3*, Bruker-AXS Inc., Madison, WI, 2016.

S3. *SADABS 2016/2*, Bruker-AXS Inc., Madison, WI, 2016.

S4. G. M. Sheldrick, *Acta Crystallogr., Sect. A: Found. Adv.*, 2015, **71**, 3–8.

S5. G. M. Sheldrick, *Acta Crystallogr., Sect. C: Struct. Chem.*, 2015, **71**, 3–8.

S6. O. V. Dolomanov, L. J. Bourhis, R. J. Gildea, J. A. K. Howard and H. Puschmann, *J. Appl. Crystallogr.*, 2009, **42**, 339–341.

S7. *TWINABS,* Bruker-AXS Inc., Madison, WI, 2016.

S8. *CELL_NOW,* G. M. Sheldrick, University of Göttingen, Germany, 2008

S9. P. van der Sluis and A. L. Spek, *Acta. Crystallogr. Sect. A: Found. Adv* 1990, **46**, 194-201

S10. L. Czepirski and J. Jagiello, *Chem. Eng. Sci.* 1989, **44**, 797-801; S. Tedds, A. Walton, D. P. Broom and D. Book, *Faraday Discuss.* 2011, **151**, 75-94